Astrofisica Nucleare e Subnucleare

“X-ray” Astrophysics

Strumentazioni per l'astrofisica

(prima parte)

Rivelazione di raggi X/γ in condizioni astronomiche

partly adapted from G. Malaguti's Lessons

Istituto Nazionale di Astrofisica (INAF) IASF-Bologna

Scanning with Slat Collimators

- Imaging the sky with non-imaging X-ray instruments as a goal
- Linear scanning means position is determined in one direction
- At least a second scanning, preferentially in the direction perpendicular to the previous one
- First all-sky survey in X-rays by Uhuru (1970-72): 2 prop. counters with metal collimators (0.5°×5°, 5°×5° FWHM)

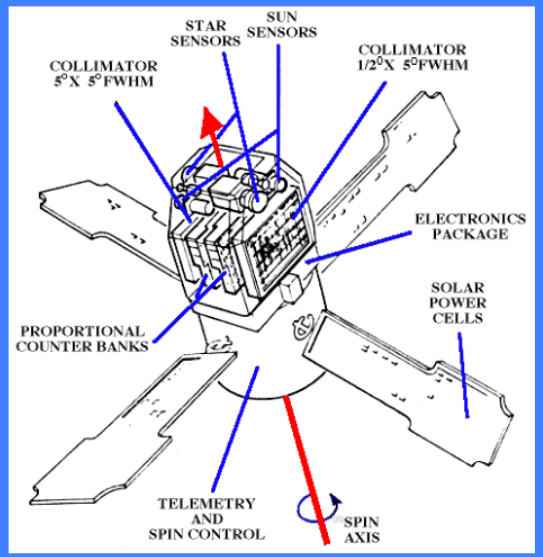

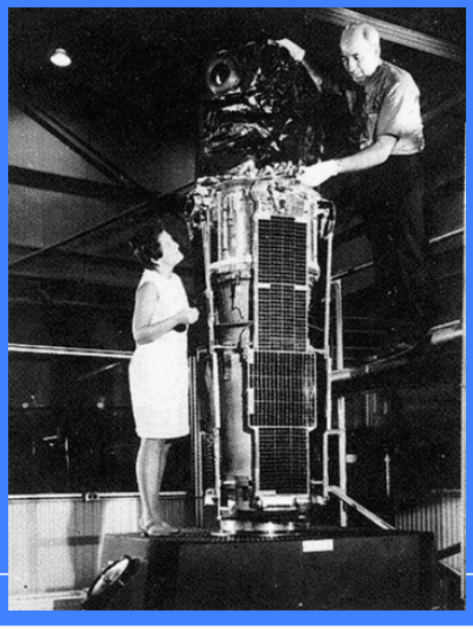

Scanning Grid Collimators

- **Two or more plane ("grid" of absorbing rods) collimators to improve angular resolution**

- **Higher resolution with three or more grids (e.g., 4 in HEAO-1 A-3 experiment)**

- **Two-dimensional measurements need scans in two or more directions**

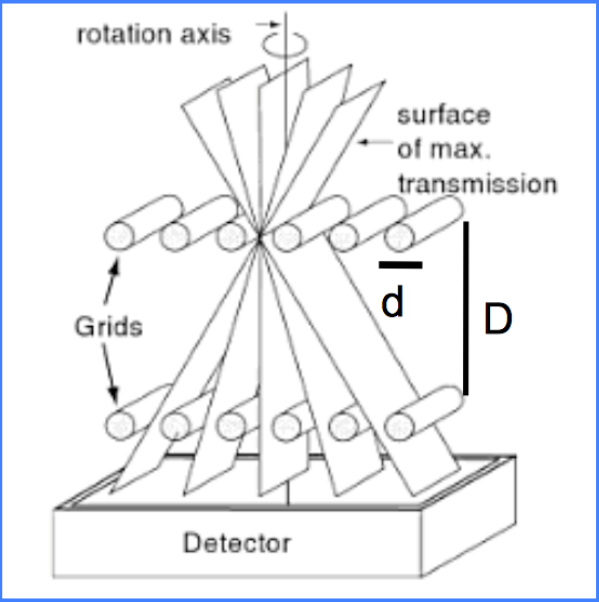

Double-grid collimator
Transmission Function of triangular shape
Angular resolution: d/D

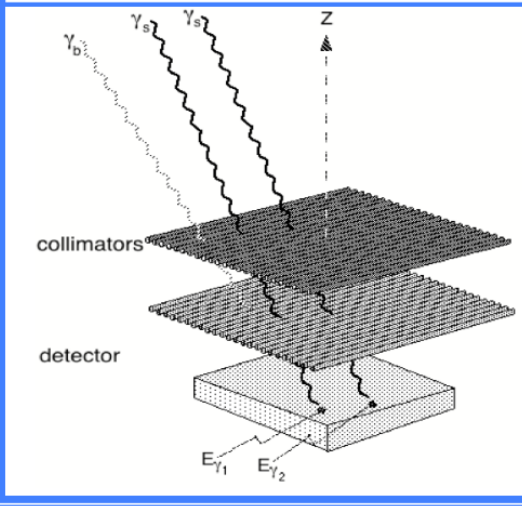

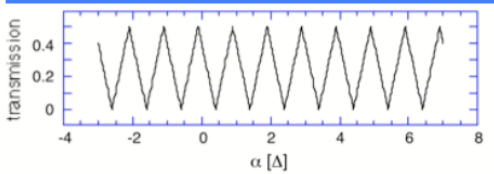

Modulation curve

Sensibilità - 1

- **Sensibilità = flusso minimo rivelabile**
  - **Emissione nel continuo: fotoni cm^{-2} s^{-1} keV^{-1}**
  - **Emissione di righe: fotoni cm^{-2} s^{-1}**
- **C_S = Tasso di conteggi di sorgente**
- **C_{Bkg} = Tasso di conteggi di fondo**

assumendo una statistica poissoniana

$$SNR = n_\sigma = \frac{C_S}{\sqrt{C_S + C_{Bkg}}}$$

In realta' quello che si misura e' (S+B)-B in un dato intervallo di tempo

$$S = (S+B) - B \longrightarrow \sigma_S^2 = \sigma_{S+B}^2 + \sigma_B^2 =$$

$$= (\sqrt{(S+B)})^2 + (\sqrt{B})^2 = S + B + B = S + 2B$$

$$SNR = S/\sigma_S = S/\sqrt{(S+2B)}$$

Sensibilità – 2 – "basic" dependencies

$S = \varepsilon\ A\ T\ \Delta E\ F_{src}$

$B = A\ T\ \Delta E\ F_{bkg}$

ε=efficienza di rivelazione fotoni della sorgente
A=area efficace
T=tempo di esposizione
ΔE=banda energetica
F_{src}=flusso della sorgente
F_{bkg}=fondo strumentale

$B << \varepsilon F_{src}$

$$SNR = \frac{S}{\sqrt{S + 2B}} \approx \sqrt{S} \propto \sqrt{F_{src} T}$$

the source dominates the signal

$B >> \varepsilon F_{src}$

$$SNR = \frac{S}{\sqrt{S + 2B}} \approx S / \sqrt{2B} \propto \sqrt{T} (F_{src} / \sqrt{2F_{bkg}})$$

Backg-dominated obsn.

$$\mathrm{SNR} = n_\sigma \approx \frac{\varepsilon \cdot \mathrm{A} \cdot \mathrm{T} \cdot \Delta\mathrm{E} \cdot \mathrm{F}}{\sqrt{\mathrm{A} \cdot \mathrm{T} \cdot \Delta\mathrm{E} \cdot \mathrm{B}}} \rightarrow F_{Min} = \frac{n_\sigma}{\varepsilon} \sqrt{\frac{B}{\mathrm{A} \cdot \mathrm{T} \cdot \Delta\mathrm{E}}}$$

to give an idea of the main dependencies of the limiting flux (sensitivity)

In the "real world", the background is not only instrumental but also cosmic

S=source flux density [counts/m^2 s]
A=area of the detector
Ω=solid angle subtended by the beam of the telescope on the sky
B_1=instrumental (particle) background [counts/s]
B_2=cosmic background (XRB) [phot/m^2 s ster]
T=exposure time
SOURCE=S×A×T (photons related to the source)
BACKGROUND=B_1×T + B_2×A×Ω×T (photons related to the backgrounds)

$$N = \sqrt{(B_1 + B_2 A\Omega) \times T}$$

$$S/N = \frac{SAT}{\sqrt{(B_1 + B_2 A\Omega) \times T}} = \frac{SA^{1/2}T^{1/2}}{\sqrt{\left(\frac{B_1}{A}\right) + \Omega B_2}}$$

$$S/N = 5 \Rightarrow S_{\min} = 5\sqrt{\frac{B_1/A + \Omega B_2}{AT}}$$

Focalizzazione vs collimazione

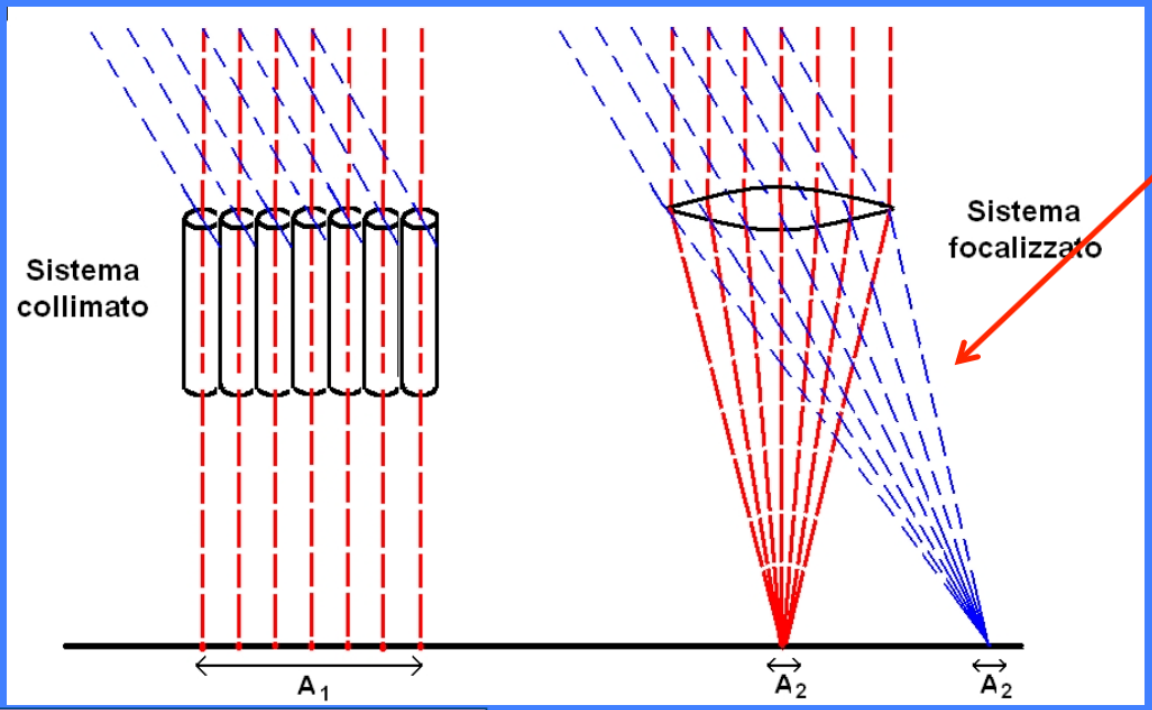

Proper imaging of X-rays below 20-40 keV

$$F_{\min} \approx n_\sigma \frac{\sqrt{2B}}{\sqrt{A_{\det} T_{\text{int}} \Delta E}}$$

A_d= PSF projected on the focal plane

$$F_{\min} \approx n_\sigma \frac{\sqrt{B A_d}}{A_{eff} \sqrt{T_{\text{int}} \Delta E}}$$

Sistema collimato: limita la regione di cielo da cui puo' provenire un segnale, (quindi limita il background), non incrementandone la "densita"

Sistema focalizzato: fa corrispondere ad ogni sorgente un punto nel piano focale, e "concentra" il segnale, producendo un' immagine

$$C_B = B\, A_d\, \Delta E\, \Delta t$$

Background counts from a collimated telescope with detector area A_d, sensitive over the band ΔE, in a time interval Δt

$$\sigma(C_B) = C_B^{1/2}$$

The counts obey the Poisson statistics

$$C_S = S_E\, A_d\, \Delta E\, \Delta t\, \eta_E$$

Source counts collected from a source with flux S_E in the same conditions (QE=η_E)

$$C_{\mathrm{meas}} = (C_S + C_B) - C_B$$

Measured counts (backg-subtracted)

$$\sigma^2(C_{\mathrm{meas}}) = 2\sigma^2(C_B)$$

Background dominates fluctuations

$$S/N = n_\sigma = \frac{C_S}{\sqrt{2C_B}} = \frac{S_E\, A_d\, \Delta E\, \Delta t\, \eta_E}{\sqrt{2B\, A_d\, \Delta E\, \Delta t}}$$

$$S_{E,\mathrm{min}} = \frac{n_\sigma}{\eta_E} \frac{\sqrt{2B}}{\sqrt{A_d\, \Delta t\, \Delta E}}$$

X-Ray Mirrors

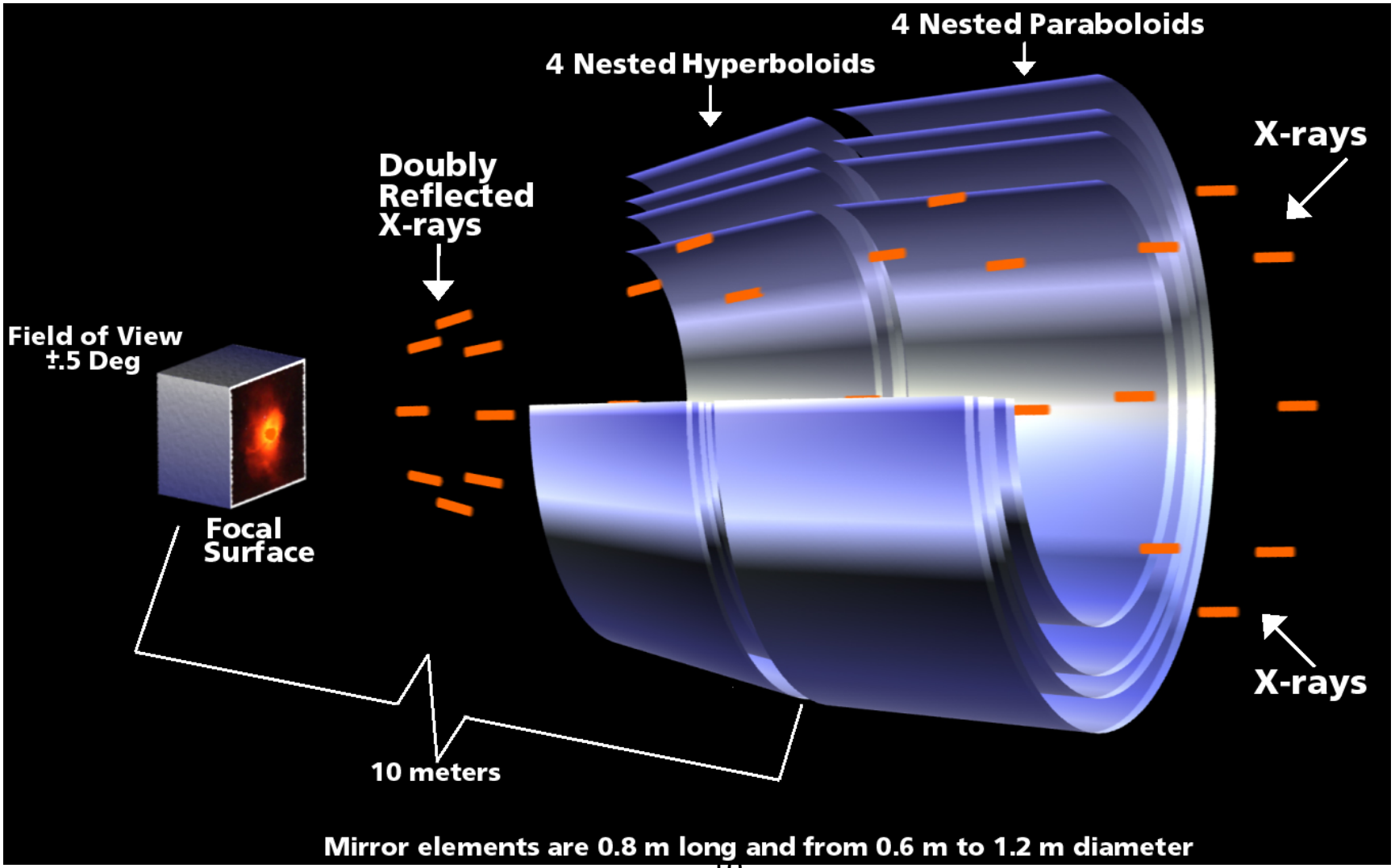

Why do we use X-ray optics

- To achieve the best 2-dim angular resolution
    - To distringuish nearby sources or different regions of the same source
    - To perform morphological studies
- As a collector to “gather” weak fluxes (case of limited photon statistics)
- As a concentrator, so that the image photons may interact in a small region of the detector, thus limiting the influence of the background
- To serve with high spectral resolution dispersive spectrometers such as transmission or reflection gratings
- To simultaneously measure both the source(s) of interest and the contaminating background in other (source-free) regions of the detector

X-ray optical constants

- X-rays are hard to refract or reflect: the refractive index of all materials in X-rays is very close to 1 and only slightly less than 1 ➔ X-rays are above the characteristic energy of bonded e- in atoms
- complex index of refraction of the reflector to describe the interaction X-rays /matter (see, for a review, Aschembach et al. 1985, Rep. Prog. Phys. 48, 579)

$$n=1-\delta+i\beta$$

where δ describes the phase change and β accounts for the absorption

δ and β depend on the wavelength

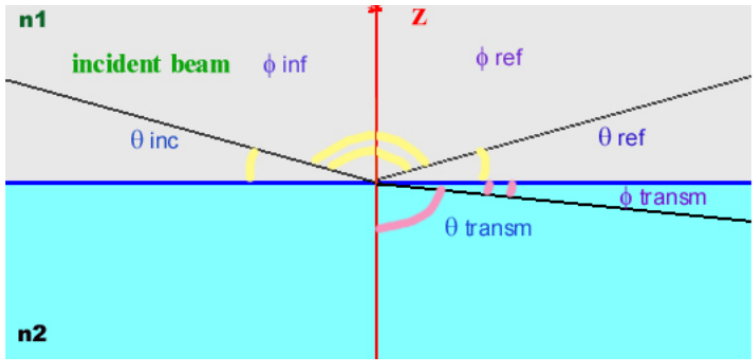

- the amplitute of reflection is described by the Fresnel's equations

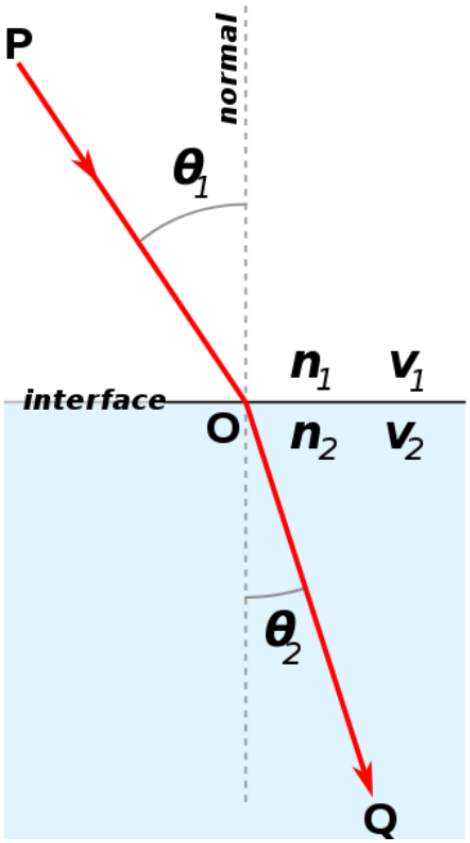

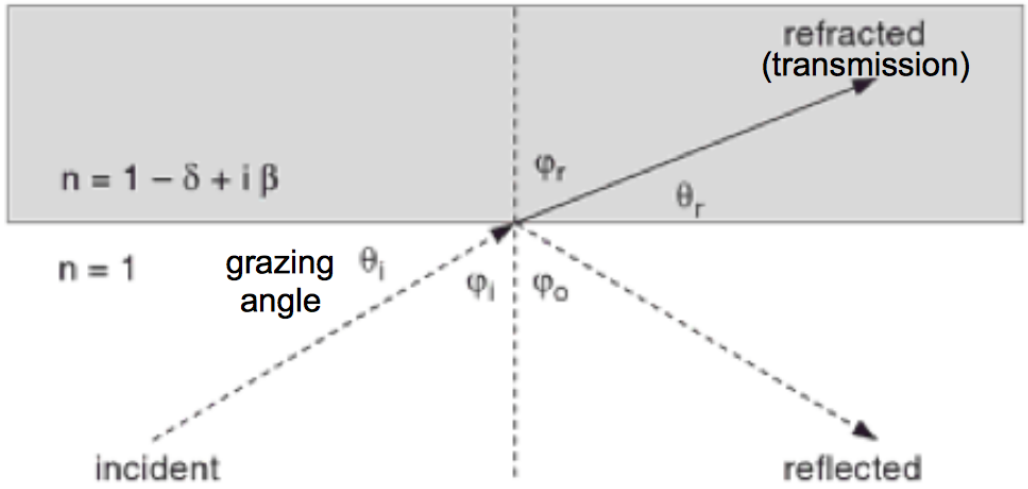

Snell's Law of Refraction:
relationship between the angles of incidence and refraction in a medium

$$n_1 \sin\theta_1 = n_2 \sin\theta_2$$

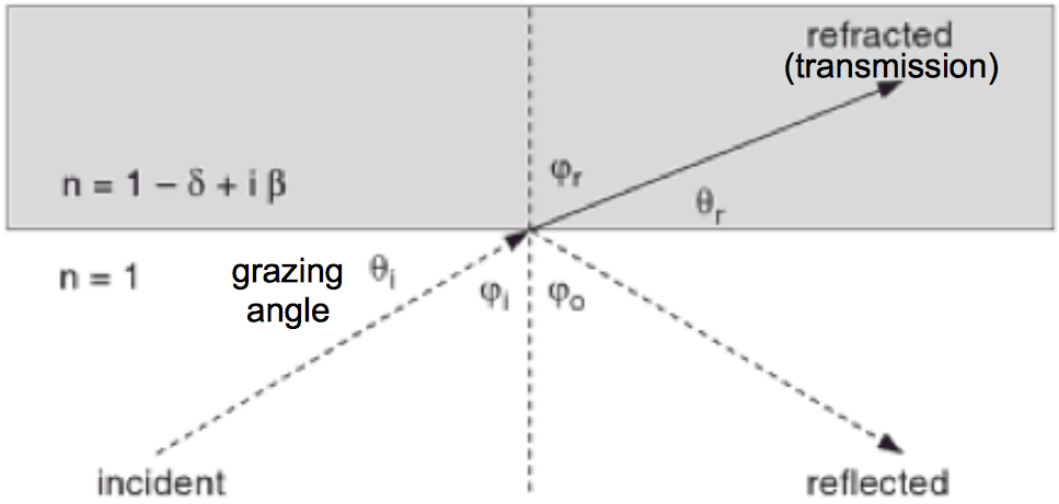

$$n_1 = 1,\ n_2 = (1-\delta) \rightarrow \sin\phi_i = (1-\delta)\sin\phi_r$$

$$\vartheta = (\pi/2) - \phi$$

$$\cos(90-\phi_i) = \cos\vartheta_i = (1-\delta)\cos(90-\phi_r) = (1-\delta)\cos\vartheta_r$$

$$\Rightarrow \cos\vartheta_i = \cos\vartheta_r(1-\delta)$$

Total reflection if no real solution for ϑ_r

$\delta>0$, $\cos\theta_r \leq 1$ ➔ There is a **critical angle θ_c** below which refraction is impossible and total external reflection occurs (grazing angle, $\theta_i=\theta_c$)

Extreme case for low θr values

$$1 = \cos\vartheta_r = \cos\vartheta_c/(1-\delta) \rightarrow \cos\vartheta_c = 1-\delta$$

Total X-ray reflection at grazing incidence

- Real part of n slightly less than unity for matter at X-rays, =1 in vacuum (total external reflection); $\delta << 1$
- Snell's law ($n1 \cos\theta_1 = n2 \cos\theta_2$) to find a critical angle for total reflection
- (Total) external reflection in vacuum for angles < critical angle: $\cos\theta_{crit} = 1 - \delta$
- X-ray partially reflected also for $\theta > \theta_{crit}$; also, some absorption in the material
- $\cos(\theta_{crit}) = 1 - \theta_{crit}^2/2 = 1 - \delta \xrightarrow{\text{low angles}} \theta_{crit} = \sqrt{2\delta}$
- Far from fluorescent edges: $\delta \approx \frac{N_0 Z r_e \rho \lambda^2}{2\pi A}$

where N_0=Avogadro's number
Z=atomic number
r_e=electron radius
ρ=density
λ=wavelength of the incoming photon
A=atomic weight

Critical angle:

- Inversely dependent on energy
- Higher Z materials reflect higher energies, for a fixed grazing angle
- Higher Z materials have a larger critical angle at any energy

- For heavy elements, Z/A≈0.5, and if δ<<1:

$$\theta_{crit} \approx \sqrt{2\delta} \approx 5.6\lambda\sqrt{\rho}$$

where λ[Å] and ρ[g/cm³], and θ[arcmin]

$$\theta_{crit} \propto \sqrt{\rho} / E$$

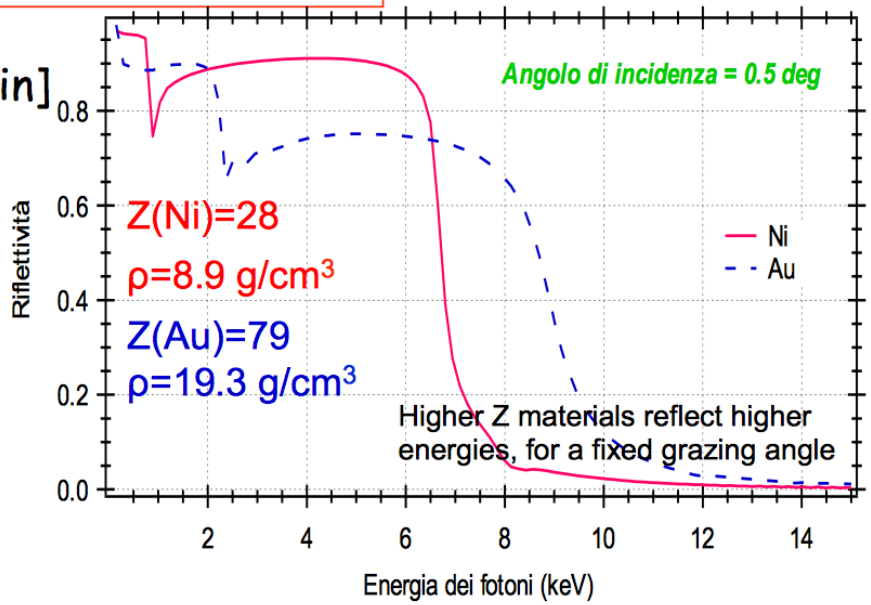

- Some reflectivity is lost due to scattering related to the presence of micro-roughness at the surface

- Use of heavy materials (but attention at the absorption edges…)

X-ray mirrors with parabolic profile

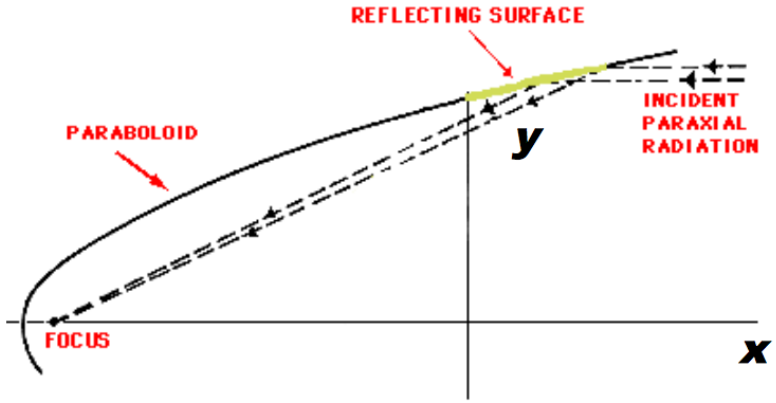

- perfect on-axis focusing
- off-axis images strongly affected by coma

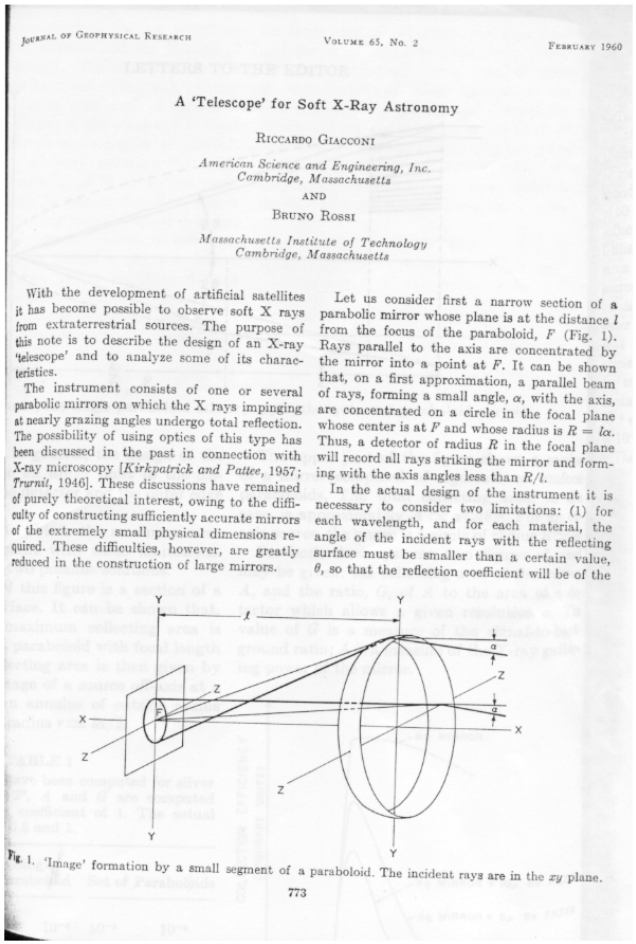

JOURNAL OF GEOPHYSICAL RESEARCH VOLUME 65, No. 2 FEBRUARY 1960

A 'Telescope' for Soft X-Ray Astronomy

RICCARDO GIACCONI

American Science and Engineering, Inc.
Cambridge, Massachusetts

AND

BRUNO ROSSI

Massachusetts Institute of Technology
Cambridge, Massachusetts

With the development of artificial satellites it has become possible to observe soft X rays from extraterrestrial sources. The purpose of this note is to describe the design of an X-ray 'telescope' and to analyze some of its characteristics.

The instrument consists of one or several parabolic mirrors on which the X rays impinging at nearly grazing angles undergo total reflection. The possibility of using optics of this type has been discussed in the past in connection with X-ray microscopy [*Kirkpatrick and Pattee*, 1957; *Trurnit*, 1946]. These discussions have remained of purely theoretical interest, owing to the difficulty of constructing sufficiently accurate mirrors of the extremely small physical dimensions required. These difficulties, however, are greatly reduced in the construction of large mirrors.

Let us consider first a narrow section of a parabolic mirror whose plane is at the distance l from the focus of the paraboloid, F (Fig. 1). Rays parallel to the axis are concentrated by the mirror into a point at F. It can be shown that, on a first approximation, a parallel beam of rays, forming a small angle, α, with the axis, are concentrated on a circle in the focal plane whose center is at F and whose radius is $R = l\alpha$. Thus, a detector of radius R in the focal plane will record all rays striking the mirror and forming with the axis angles less than R/l.

In the actual design of the instrument it is necessary to consider two limitations: (1) for each wavelength, and for each material, the angle of the incident rays with the reflecting surface must be smaller than a certain value, θ, so that the reflection coefficient will be of the

Fig. 1. 'Image' formation by a small segment of a paraboloid. The incident rays are in the xy plane.

773

Wolter, 1952

Wolter's solution to the X-ray imaging

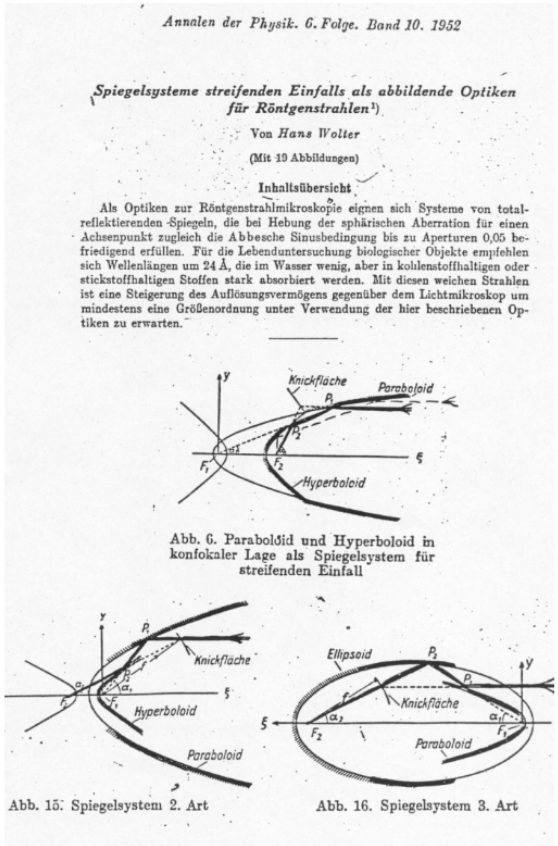

Annalen der Physik. 6. Folge. Band 10. 1952

Spiegelsysteme streifenden Einfalls als abbildende Optiken für Röntgenstrahlen[1])

Von *Hans Wolter*

(Mit 19 Abbildungen)

Inhaltsübersicht

Als Optiken zur Röntgenstrahlmikroskopie eignen sich Systeme von totalreflektierenden Spiegeln, die bei Hebung der sphärischen Aberration für einen Achsenpunkt zugleich die Abbesche Sinusbedingung bis zu Aperturen 0,05 befriedigend erfüllen. Für die Lebenduntersuchung biologischer Objekte empfehlen sich Wellenlängen um 24 Å, die im Wasser wenig, aber in kohlenstoffhaltigen oder stickstoffhaltigen Stoffen stark absorbiert werden. Mit diesen weichen Strahlen ist eine Steigerung des Auflösungsvermögens gegenüber dem Lichtmikroskop um mindestens eine Größenordnung unter Verwendung der hier beschriebenen Optiken zu erwarten.

Abb. 6. Paraboloid und Hyperboloid in konfokaler Lage als Spiegelsystem für streifenden Einfall

Abb. 15. Spiegelsystem 2. Art

Abb. 16. Spiegelsystem 3. Art

Fine for X-ray astronomy **a**

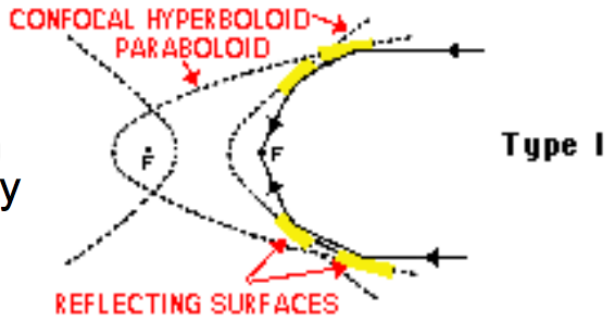

Applied in solar X-ray telescopes **b**

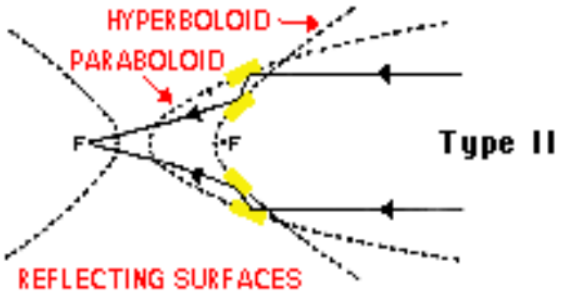

Not adopted **c**

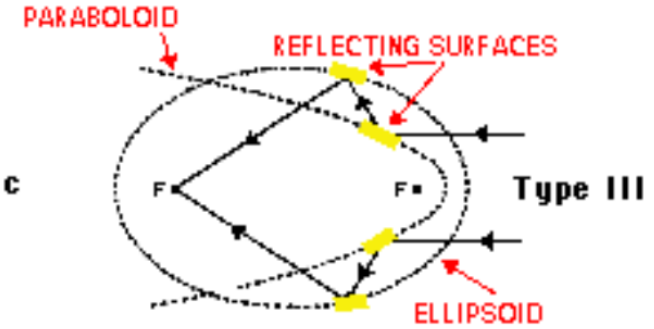

H. Wolter, Ann. Der Phys., NY10, 94 (1952)

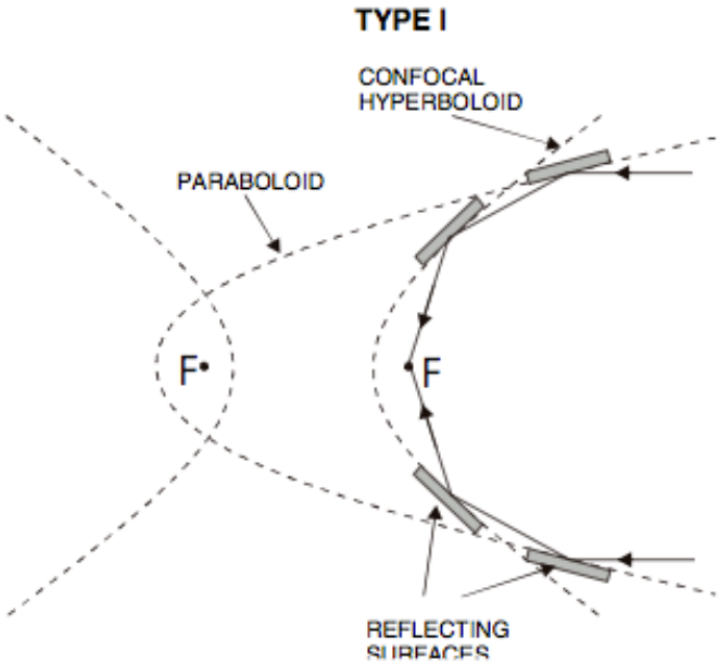

Wolter-I optics

Paraboloid ➔ Hyperboloid

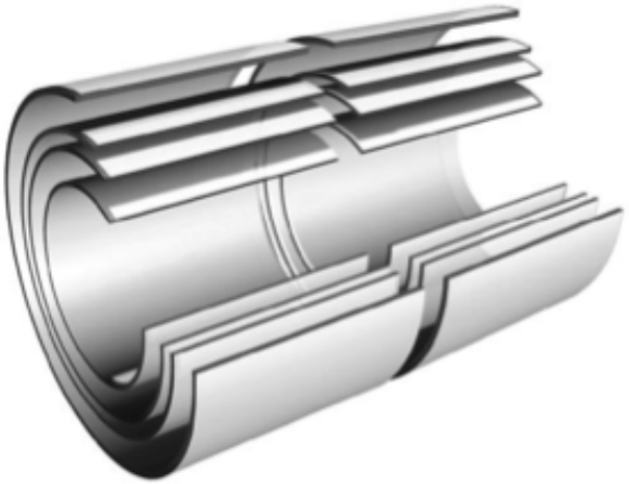

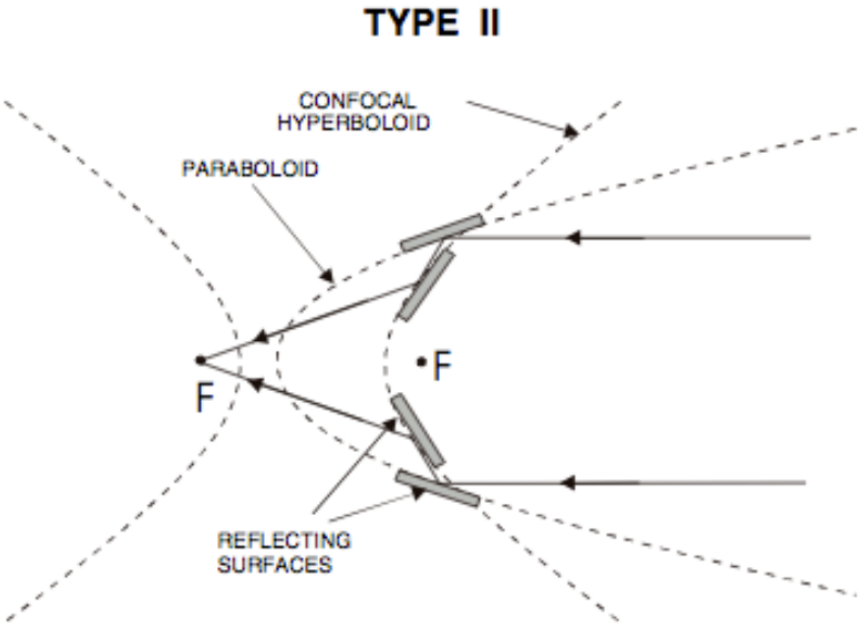

Wolter-II optics

Paraboloid ➔ Hyperboloid (ext. surface)

X-Ray Mirrors

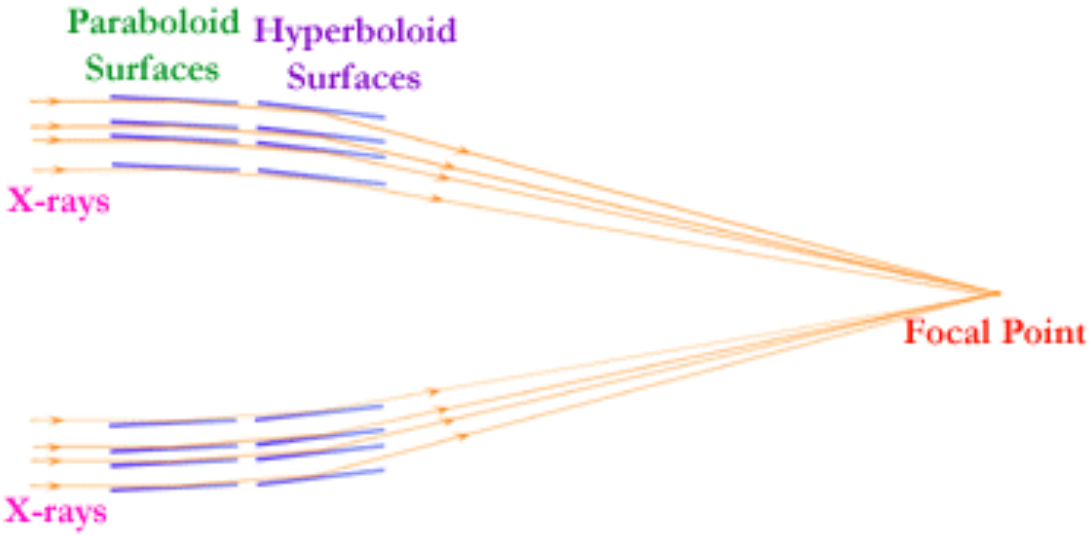

$$\cos\phi = 1 - \delta$$

$$\delta = 2.70 \times 10^{-6} \frac{Z_e}{A} \rho\lambda^2$$

Cf Aschembach et al. 1985

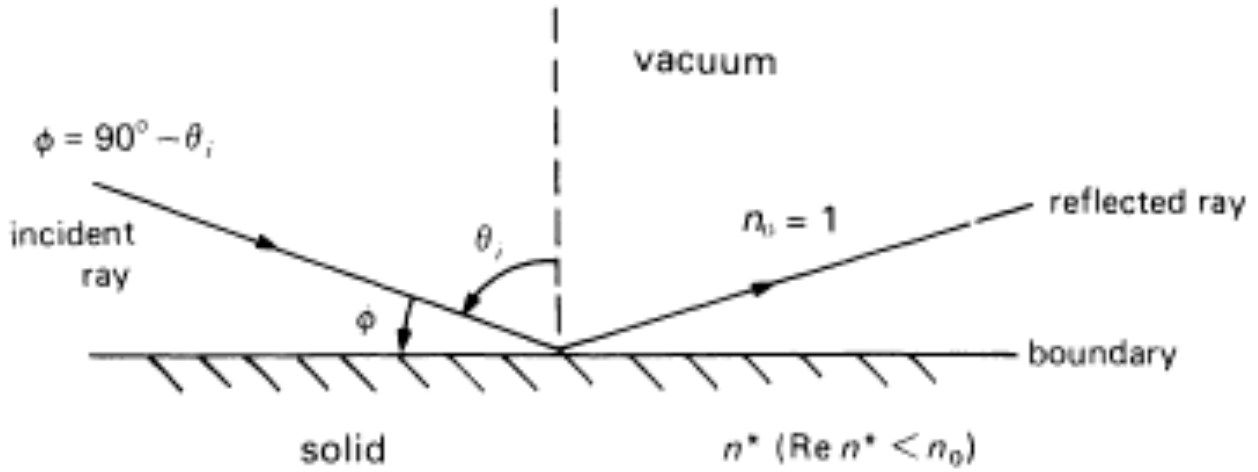

A_{geom} x Reflectivity

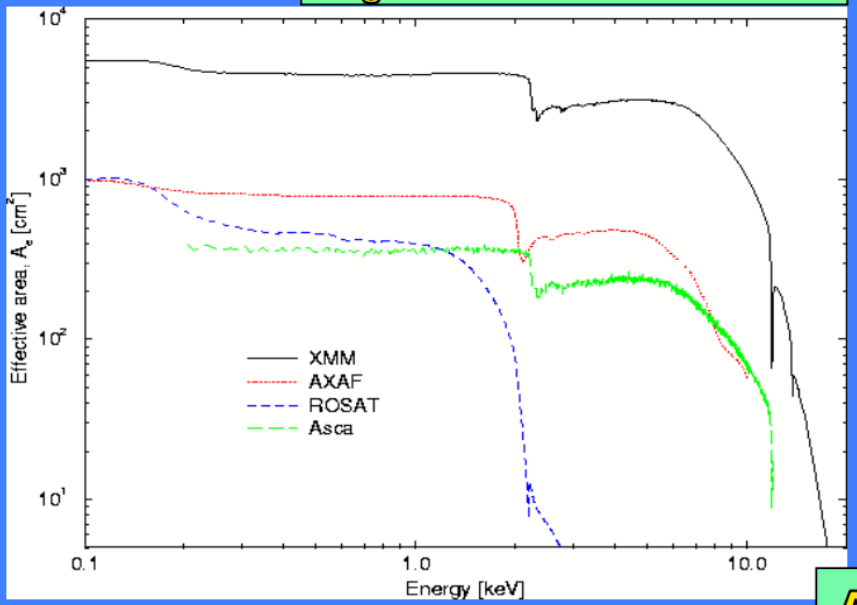

x

QE

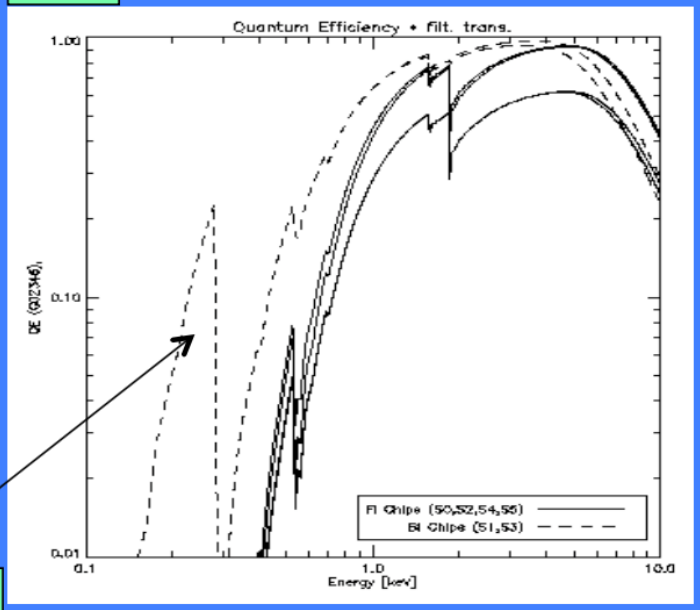

$A_{effective}$

=

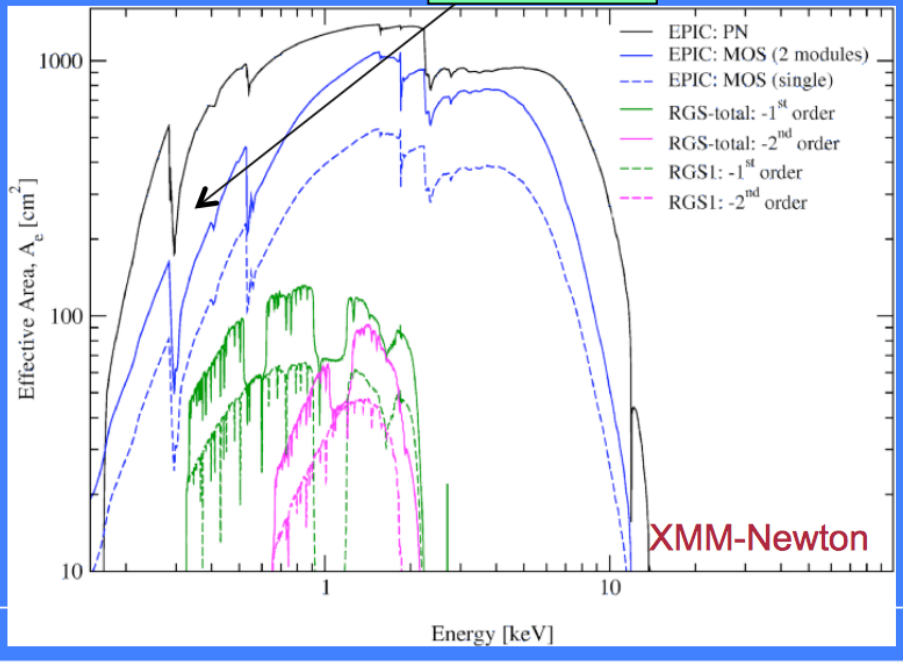

CCD

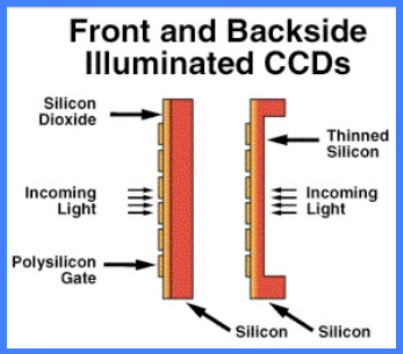

Focalizzazione vs collimazione

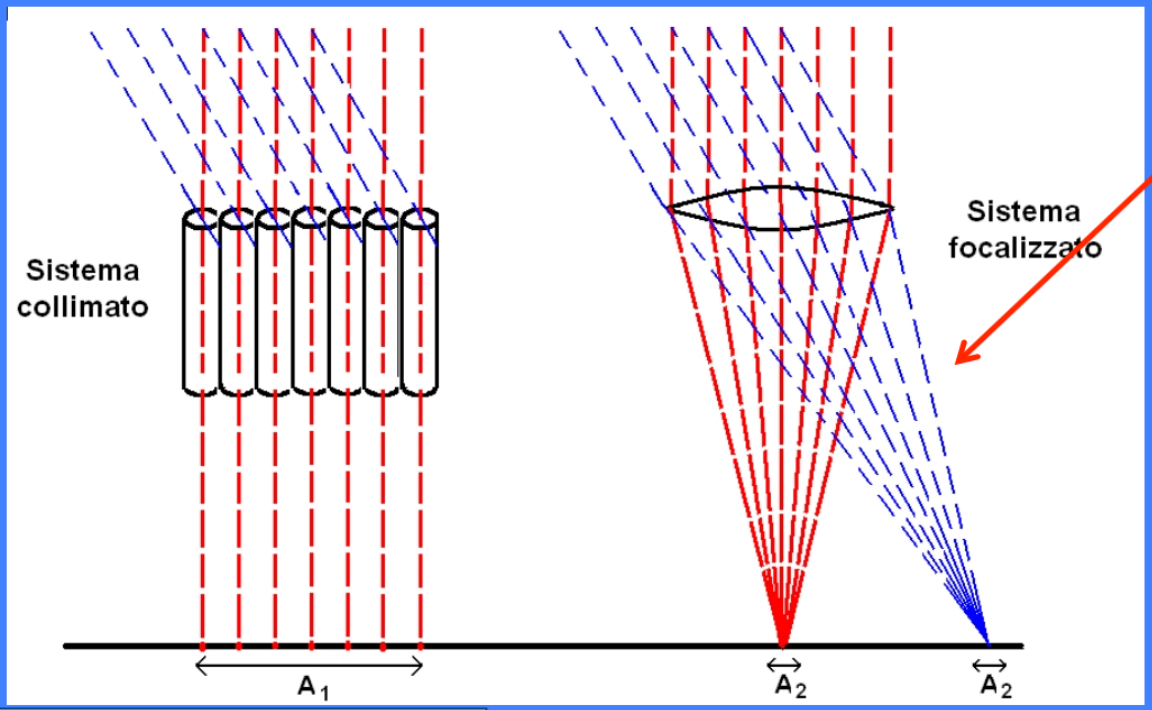

Proper imaging of X-rays below 20-40 keV

$$F_{\min} \approx n_\sigma \frac{\sqrt{2B}}{\sqrt{A_{\det} T_{\text{int}} \Delta E}}$$

A_d= PSF projected on the focal plane

$$F_{\min} \approx n_\sigma \frac{\sqrt{B A_d}}{A_{eff} \sqrt{T_{\text{int}} \Delta E}}$$

Sistema collimato: limita la regione di cielo da cui puo' provenire un segnale, (quindi limita il background), non incrementandone la "densita"

Sistema focalizzato: fa corrispondere ad ogni sorgente un punto nel piano focale, e "concentra" il segnale, producendo un' immagine

$$C_S = S_E \, A_e \, \Delta E \, \Delta t \, \eta_E$$

Detected signal

$$C_B = B \, \varepsilon \, A_d \, \Delta E \, \Delta t$$

Background signal (ε: region of the detector where B counts are focused)

$$S/N = n_\sigma = \frac{C_S}{\sqrt{C_S + 2C_B}} \approx \frac{S_E \, A_e \, \Delta E \, \Delta t \, \eta_E}{\sqrt{2B \, \varepsilon \, A_d \, \Delta E \, \Delta t}}$$

$$S_{E,\min} = \frac{n_\sigma}{\eta_E} \, \frac{1}{A_e} \sqrt{\frac{2B \, \varepsilon \, A_d}{\Delta t \, \Delta E}}$$

Weak sources

Old slide but *Chandra* and XMM-*Newton* still working

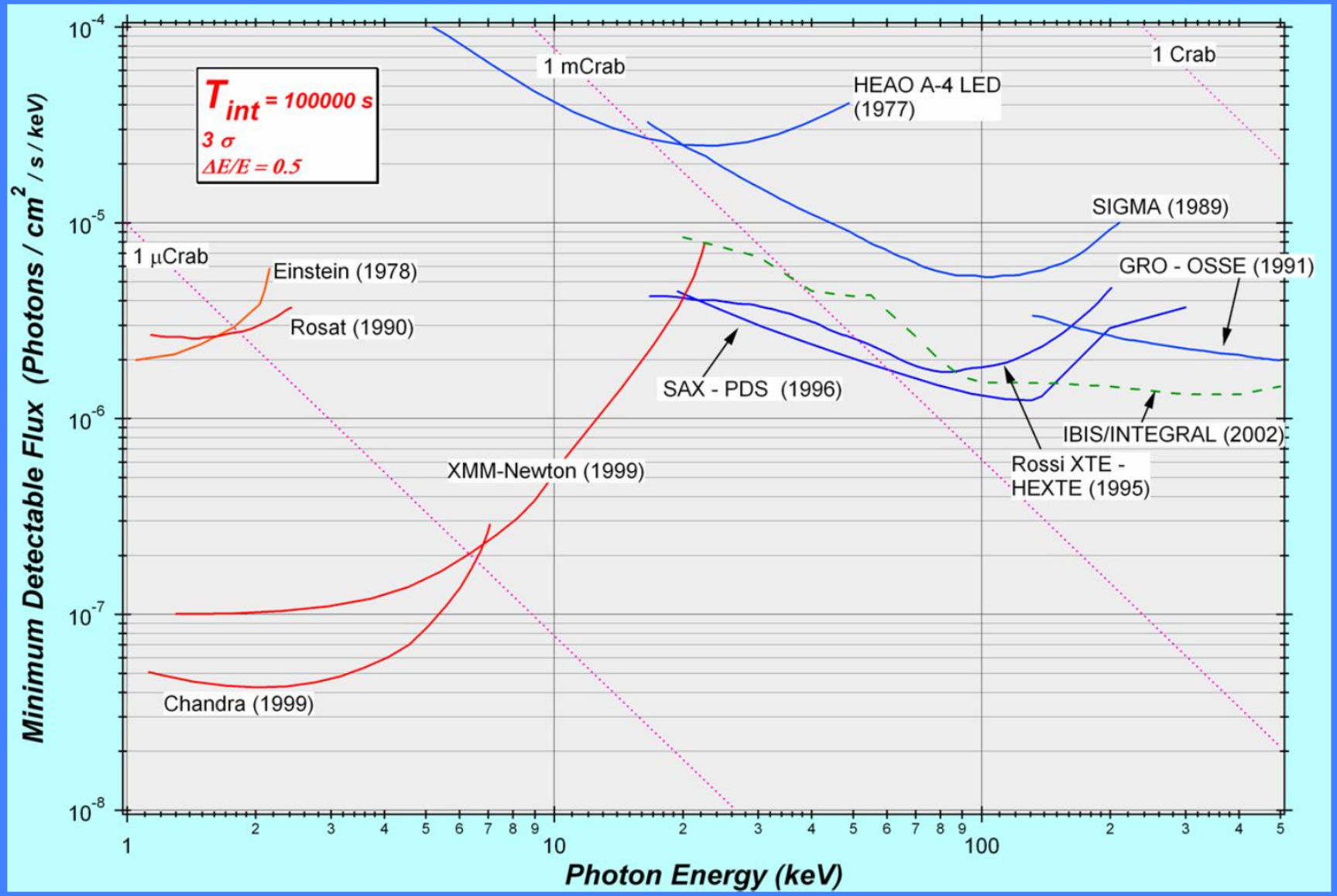

Single photon calorimeter

Individual X-ray photons are absorbed by a crystal which is maintained at a T very close to absolute zero (<0.1 K).
➔ 2-3 year lifetime

We measure the increase of T which is proportional to the energy of the X-ray photon

Energy resolution ~ 3 eV

High efficiency

The best spectral resolution of any non-dispersive (grating) spectrometer

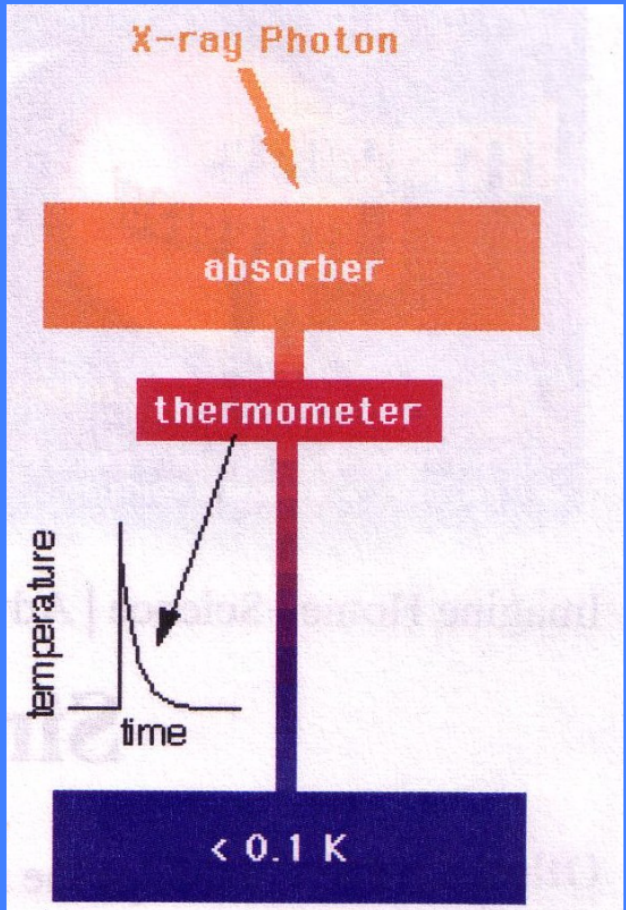

Diagram showing the essential elements of a calorimeter. Inset shows temperature response to an X-ray hit.

Onboard *Suzaku* – calibration source (^{55}Fe)

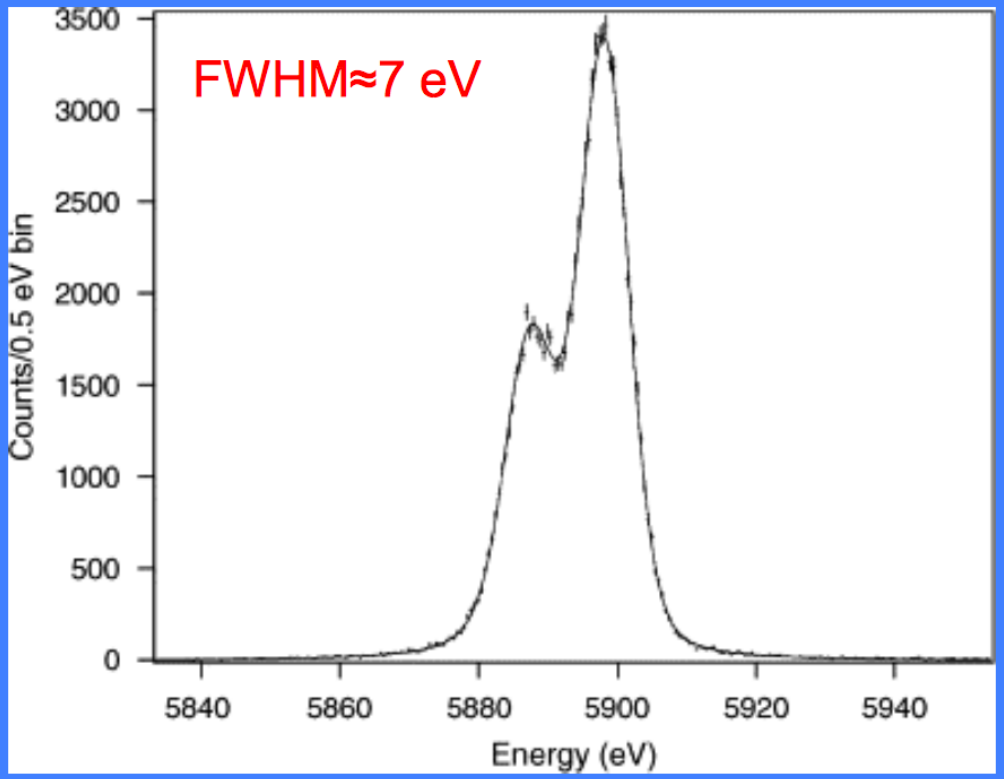

Expected spectral resolutions ≤2-3 eV in next-generation X-ray calorimeters (e.g., *Athena*)

Onboard of the Japanese mission ASTRO-H/*Hitomi* (

Last year ☹

)

X-ray spectroscopy

Telescopes and instruments

Dispersing elements – Bragg Crystal spectroscopy/1

(more details on dispersive spectrometers: Giacconi & Gursky, p. 81-90)

The reflection of X-rays from a crystal lattice follows the Bragg's law, and therefore the name Bragg spectrometer is usually given to the device with this kind of reflection grating.

Here the macroscopic shaping (grooves) of a metallic plate, which is used in longer wavelengths, is replaced by a material with regular lattice structure of atoms (crystal material). The reflection takes place by the same principle as from a macroscopic lattice, leading to a wavelength-dispersed output from a white light input.

The lattice of the crystal forms a 3-dimensional diffraction array which reflects X-rays of wavelength λ within a narrow range of wavelength satisfying the Bragg condition

$$n\lambda = 2d\sin\theta \quad , n = 1,2,3,\ldots \text{ (order of diffraction)}$$

where *d* is the crystal lattice spacing.
In practice, order n=1 is used.

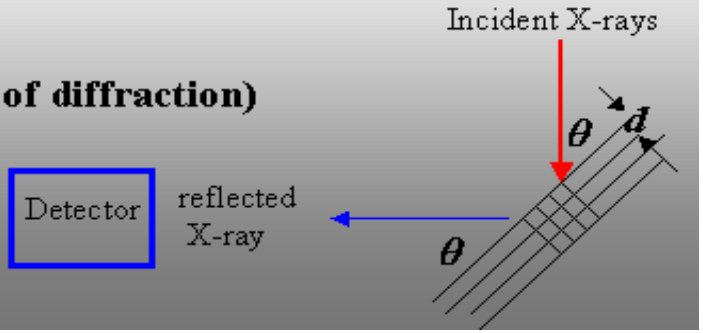

X-ray spectroscopy

Dispersing elements – Diffraction gratings/1

Ordinary diffraction gratings can also be used from from long wavelengths up to soft X-rays (< 1 keV, in practice).

The grating equation is

$$n\,\lambda = (1/N)\ (\sin\theta - \sin\theta_o),\ \ n = 1,2,3,\ldots \text{ (order of diffraction)}$$

where N is the grating constant (lines/cm), θ is the diffraction angle and θ_o is the angle of incidence. For X-rays this is usually rearranged in form valid for small angles

$$n\,\lambda\,N = \theta - \theta_o$$

There are two geometries usually applied in X-ray optics,

1. Conventional Johann mount geometry

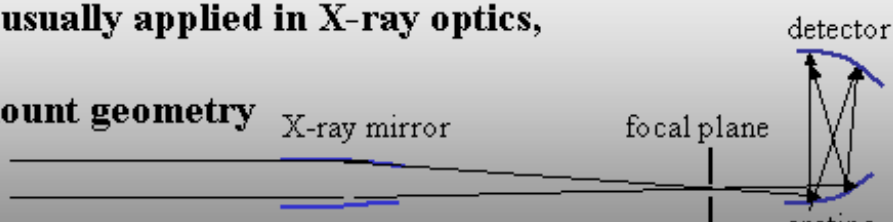

2. Curved grating producing a line image

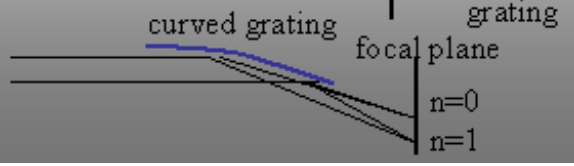

X-ray polarimetry

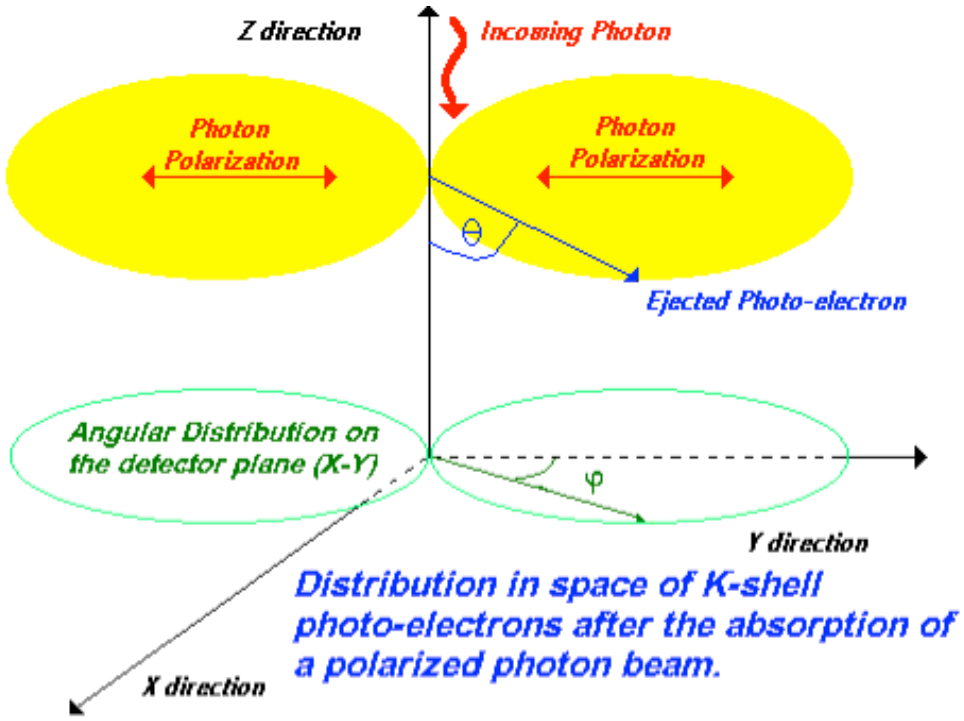

Costa et al. 2001

X-ray polarimetry

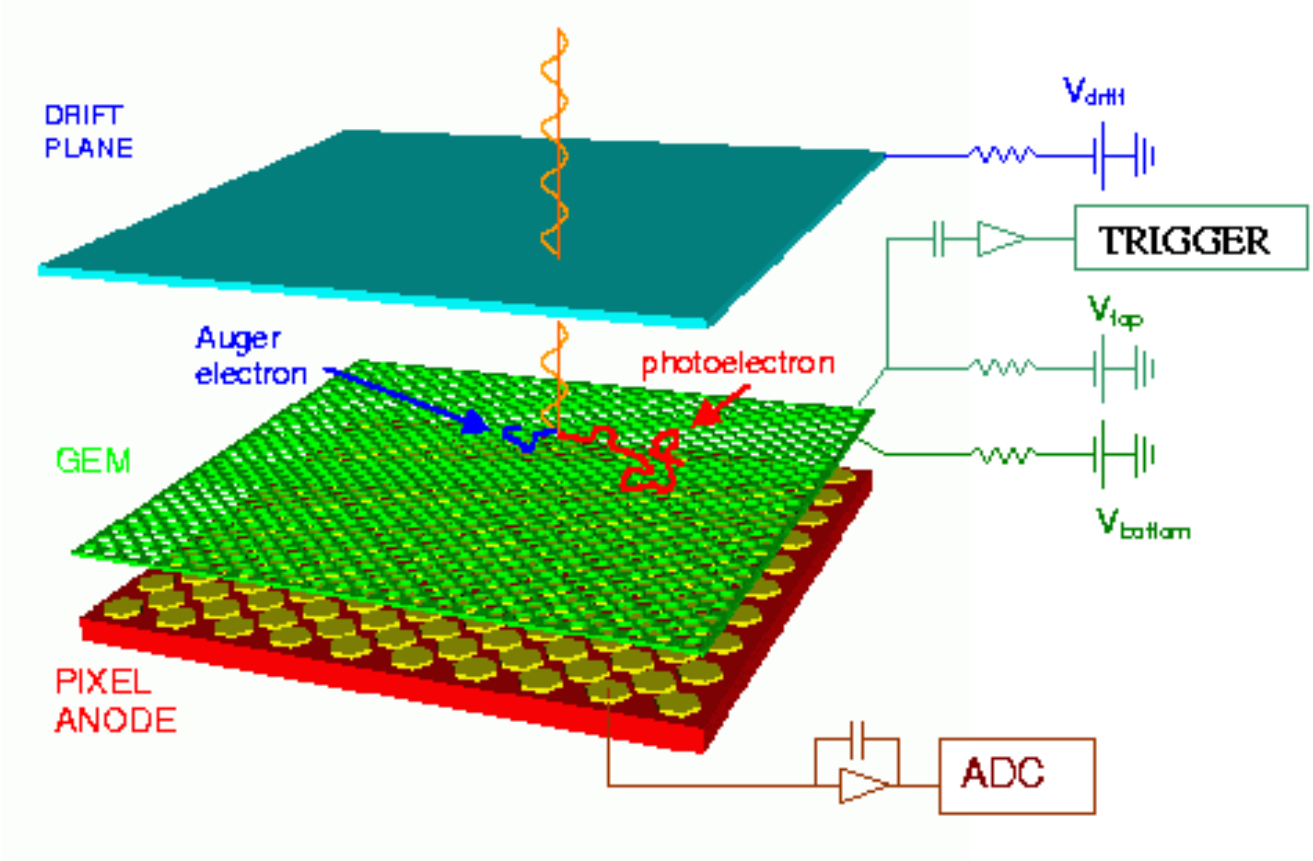

X-ray imaging

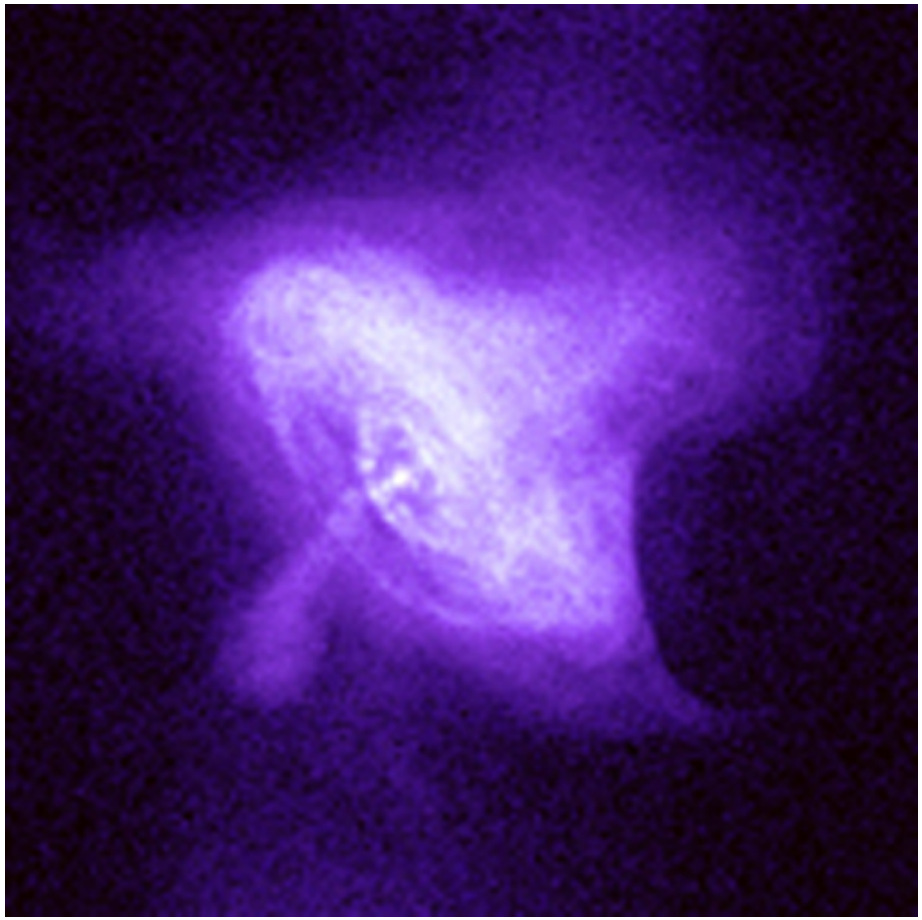

Crab nebula, 2.5”, 0.3 – 3 keV

La risoluzione angolare in astronomia X: da *ROSAT* a *Chandra*

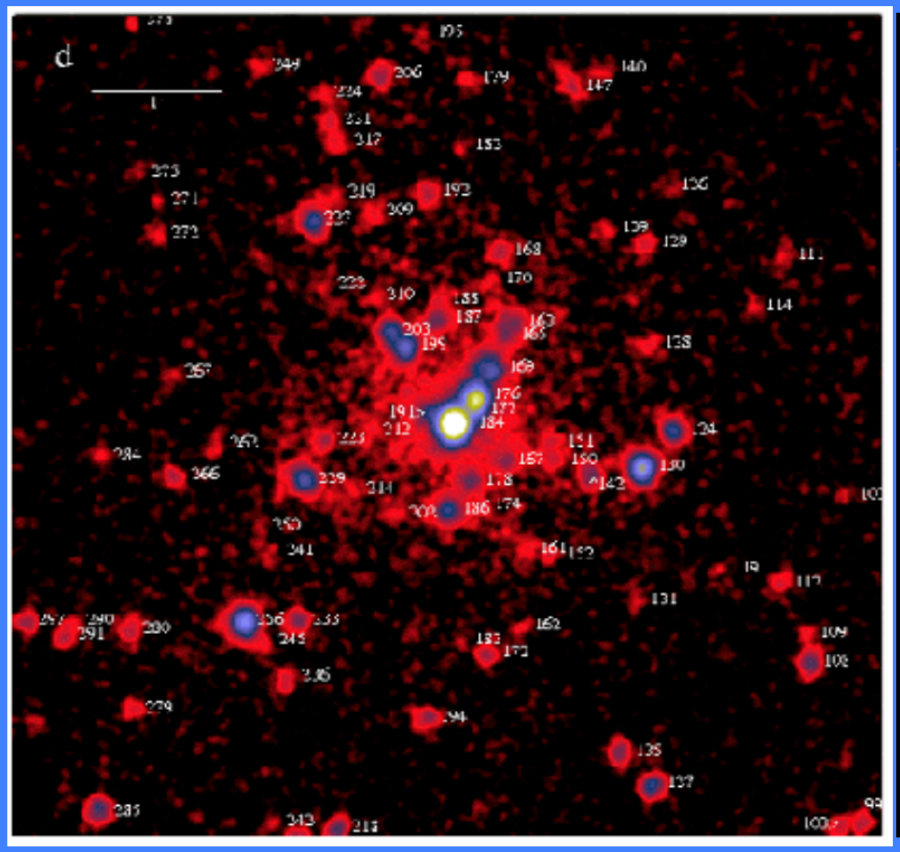

Osservazione di Orion
con ROSAT HRI (47 ks)

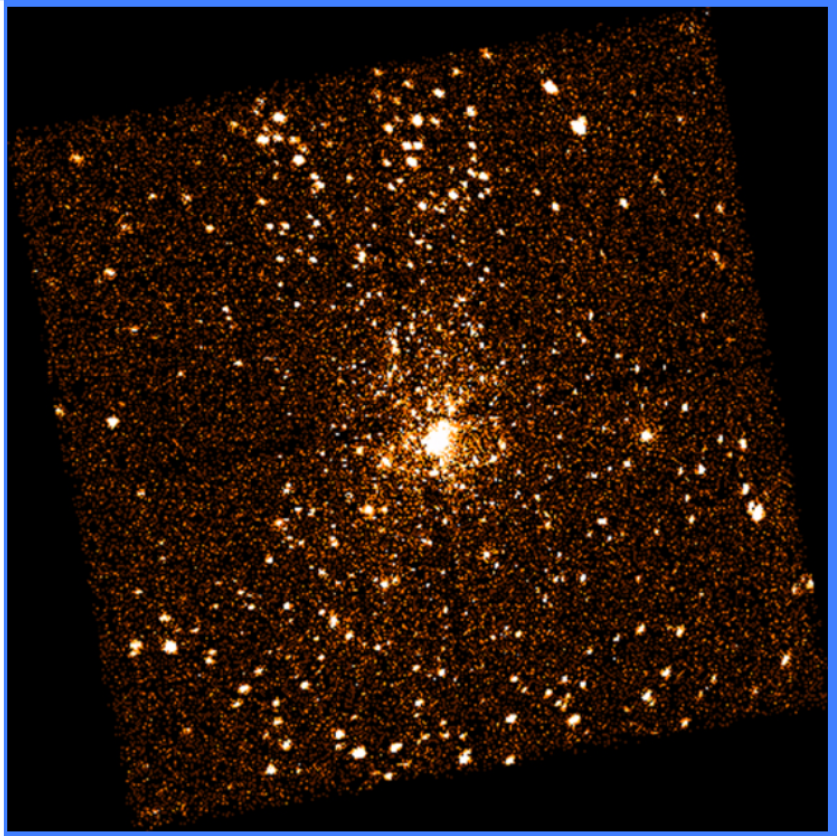

Osservazione di Orion
con Chandra ACIS (13.7 ks)

X-ray spectroscopy

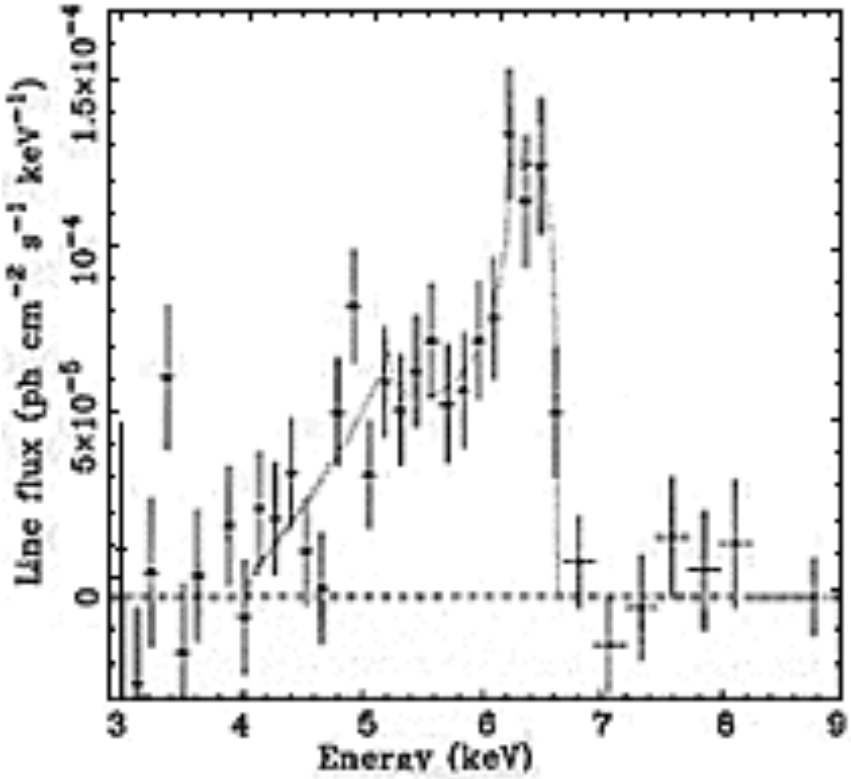

The Fe line profile of K-alpha in the X-ray emission from the active nucleus of the galaxy MCG 6-30-15 in the constellation Centaurs is powered by matter accreting into a black hole.

ROSAT results

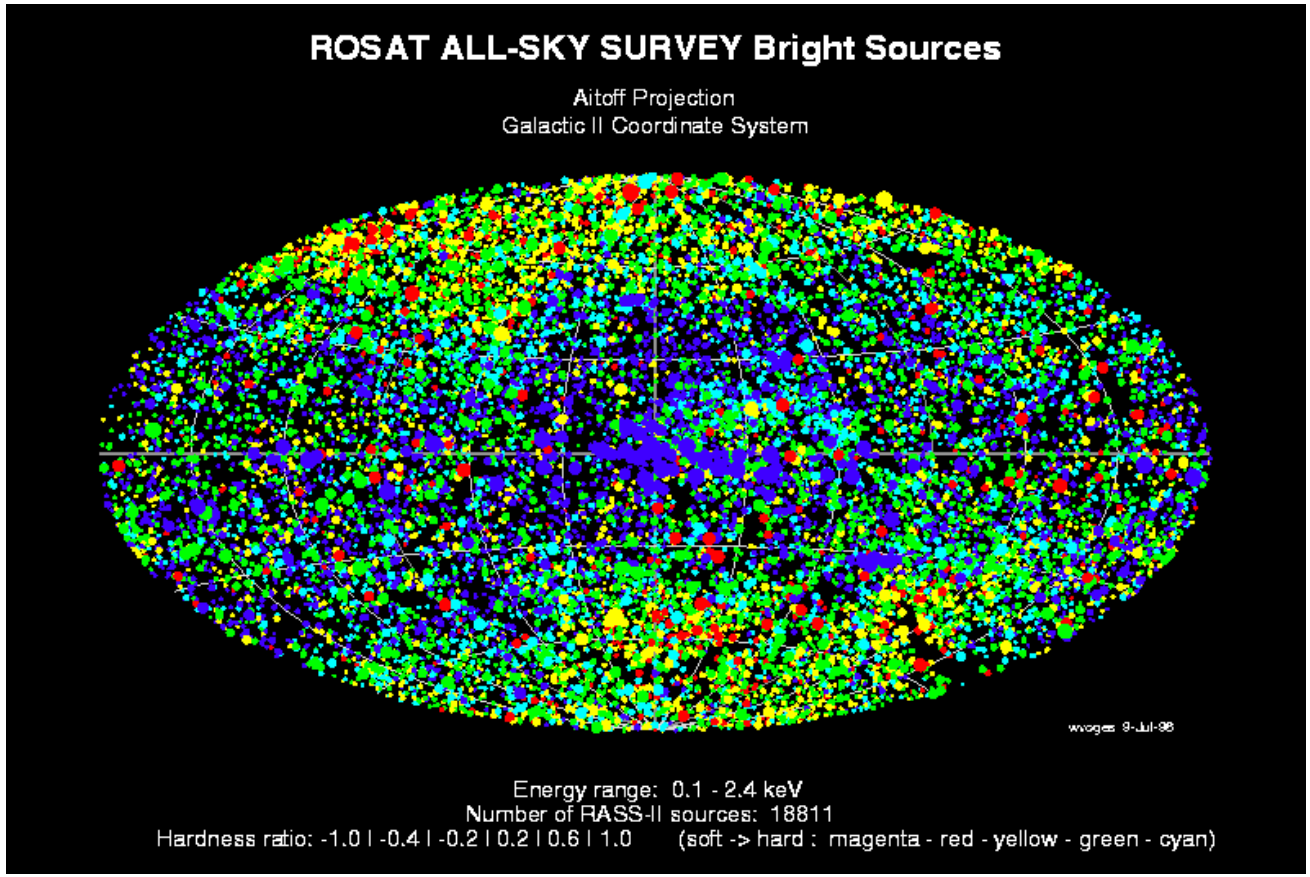

The ROSAT All-Sky Survey Bright Source Catalogue (RASS-BSC, revision 1RXS) is derived from the all-sky survey performed during the first half year of the ROSAT mission in 1990/91. 18,811 sources are catalogued, with a limiting ROSAT PSPC countrate of 0.05 cts/s in the 0.1-2.4 keV energy band. 34

ROSAT http://www.mpe.mpg.de/xray/wave/rosat/

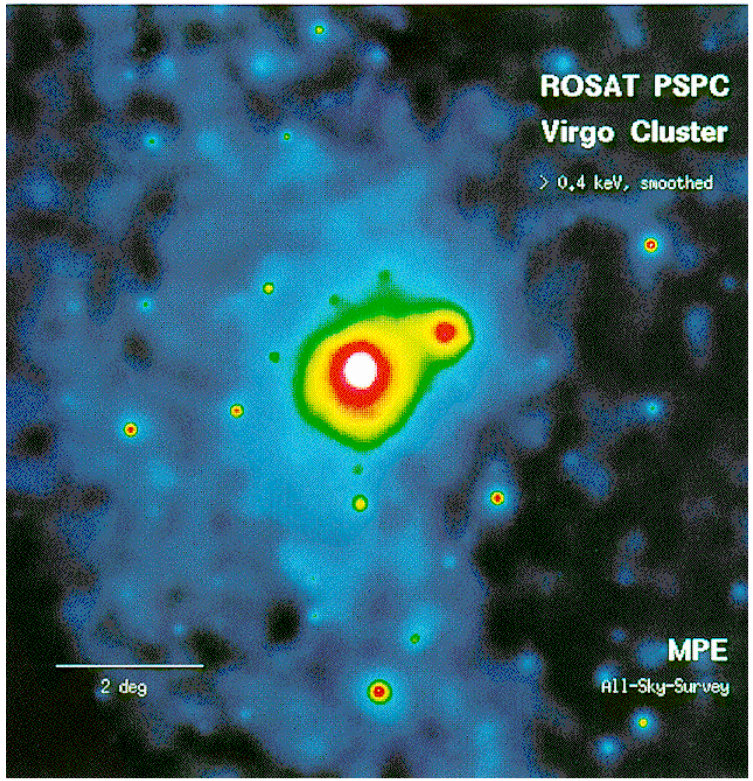

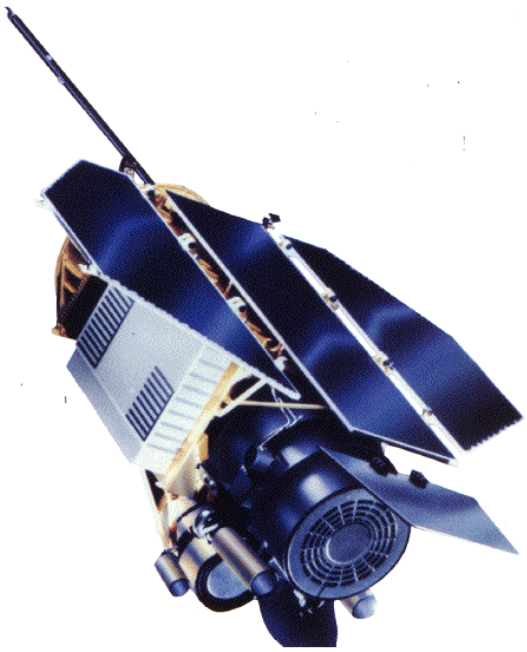

The scientific payload consists two coalligned scientific experiments, the The X-Ray Telescope which is used in conjunction with one of the focal plane instruments:

- The Position Sensitive Proportional Counter
- The High Resolution Imager

and the The Wide Field Camera which has its own mirror system and star sensor.

ROSAT provides a ~ 2 degree diameter field of view with the PSPC in the focal plane, and ~ 40 arcmin diameter field of view with the HRI in the focal plane. The ROSAT mission began with a six-month, all-sky PSPC survey, after which the satellite began a series of pointed observations that continued for the duration of the project.

ROSAT results

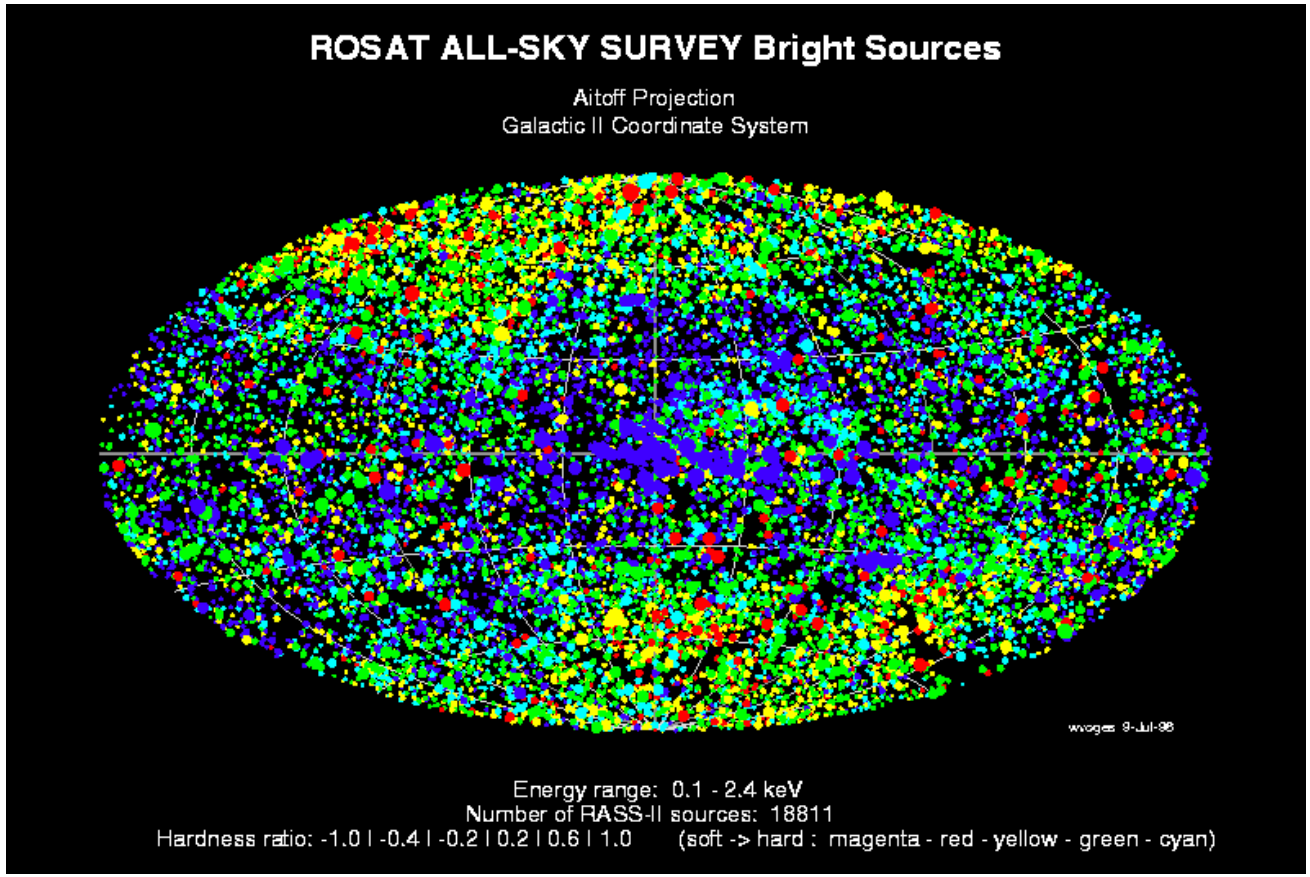

The ROSAT All-Sky Survey Bright Source Catalogue (RASS-BSC, revision 1RXS) is derived from the all-sky survey performed during the first half year of the ROSAT mission in 1990/91. 18,811 sources are catalogued, with a limiting ROSAT PSPC countrate of 0.05 cts/s in the 0.1-2.4 keV energy band.

RXTE http://heasarc.gsfc.nasa.gov/docs/xte/xtegof.html

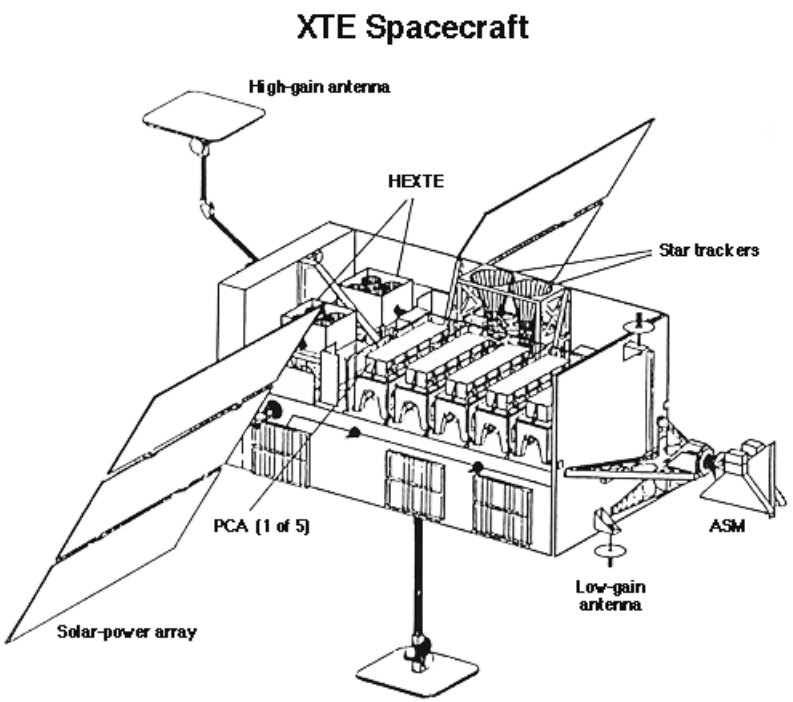

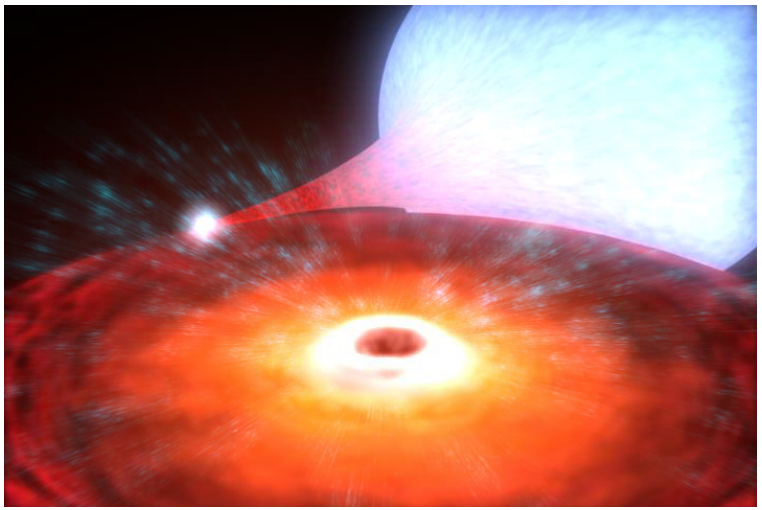

The lowest-mass known black hole belongs to a binary system named XTE J1650-500. The black hole has about 3.8 times the mass of our sun, and is orbited by a companion star

The Rossi X-ray Timing Explorer (RXTE) was launched on December 30, 1995.
RXTE features unprecedented time resolution in combination with moderate spectral resolution to explore the variability of X-ray sources. Time scales from microseconds to months are covered in an instantaneous spectral range from 2 to 250 keV.
Originally designed for a required lifetime of two years with a goal of five, it operated up to 2012

BeppoSAX

http://www.asdc.asi.it/bepposax

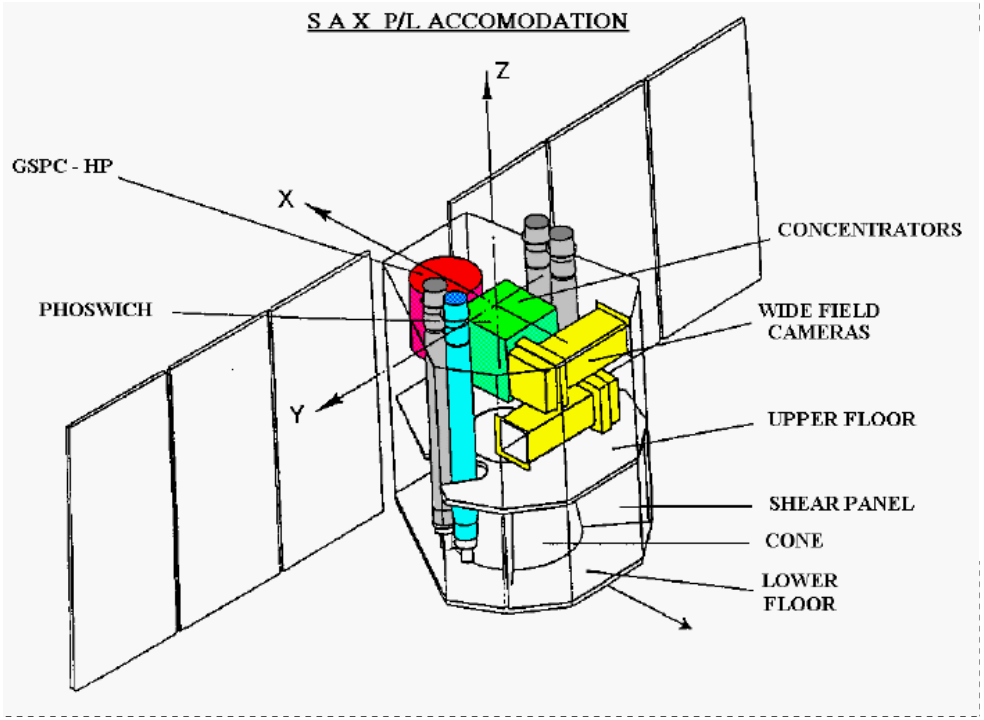

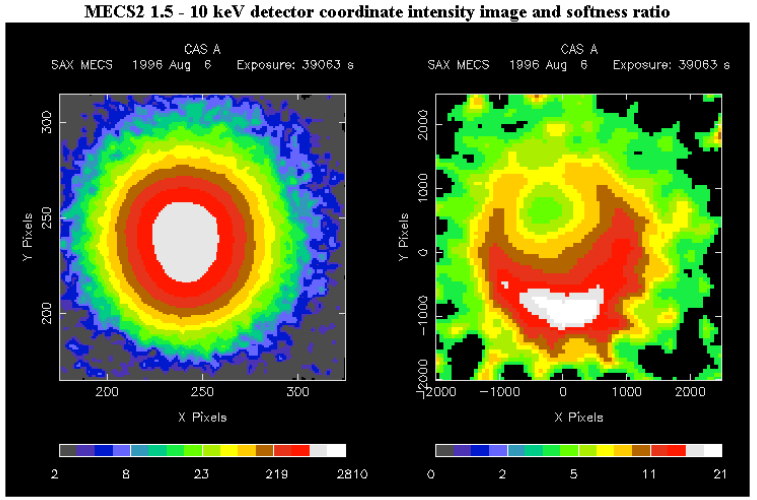

- **Energy Range 0.1 to 200 keV**
- **Imaging capabilities (1') in the range of 0.1-10 keV.**
- **High energy (3-300 keV)**
- **Narrow fields and point in the same direction (Narrow Field Instruments, NFI).**
- **Monitoring large regions of the sky with a resolution of 5' in the range 2-30 keV**
  - two coded mask proportional counters pointing in diametrically opposed directions perpendicular to the NFI
- **Anticoincidence scintillator shields of the PDS will be used as a gamma-ray burst monitor in the range 60-600 keV.**

BeppoSAX results

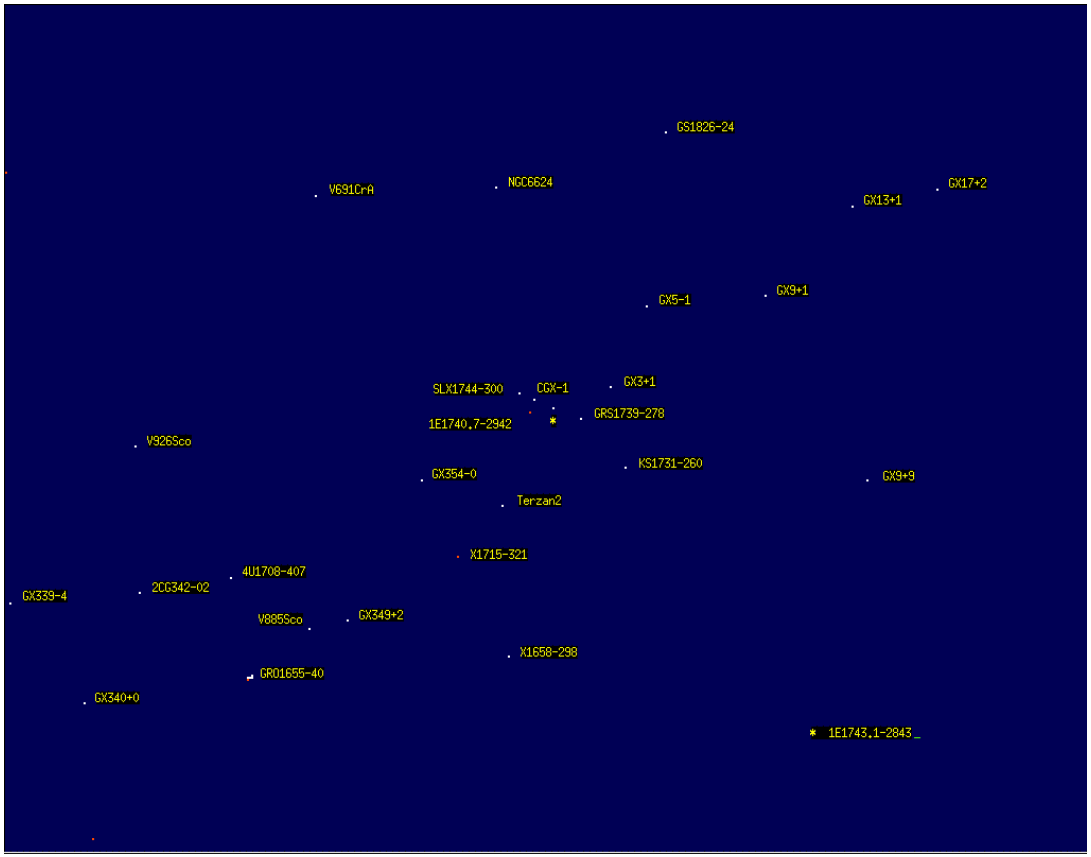

The Galactic Centre has been observed with the Beppo SAX Wide Field Camera 1 (WFC1) in August 1996.
Here an image is shown of the 40 degrees by 40. The observation period was from 22-8-1996 07.54 UT through to 23-8-1996 11.38 UT, while the effective exposure totalled about 51 kiloseconds. The number of accepted events was 1.7955 x 10^7 in the energy range of 5.4 - 11.3 keV. The legenda for the galactic centre source indicated with a yellow star (1E1743.1-2843), is given at lower right in the image.

To our knowledge this is the largest field ever imaged in X-rays in a single pointing.

Chandra X-ray Telescope

http://chandra.harvard.edu/

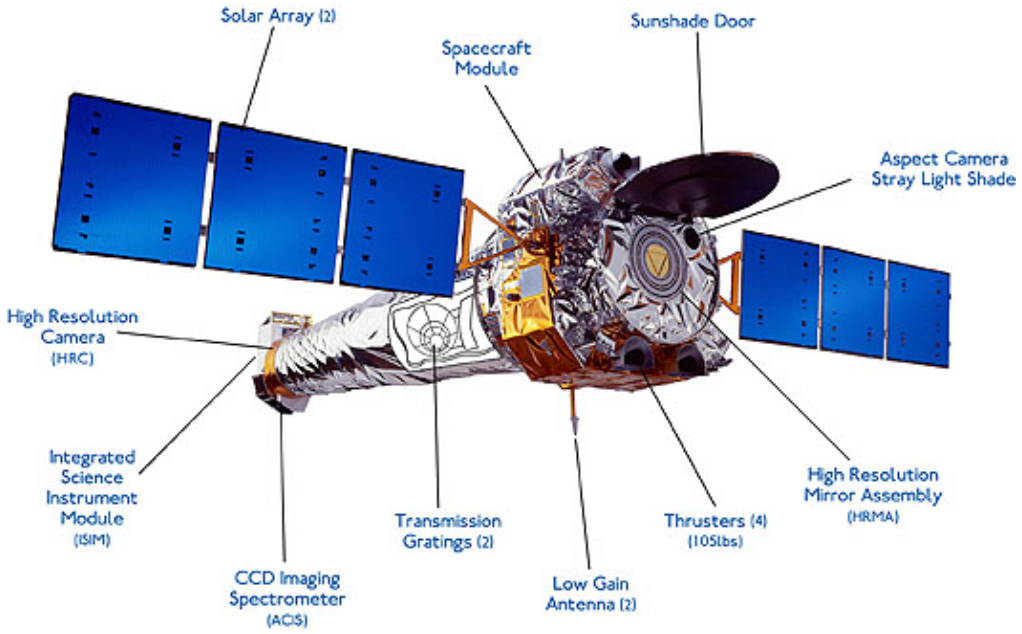

High resolution mirror
two imaging detectors
two sets of transmission gratings.
Spatial resolution: 0.5”
Good sensitivity from 0.1 to 10 keV
High spectral resolution $E/\Delta E = 1000$

XMM-Newton

http://sci.esa.int/xmm-newton/

XMM carries the X-ray telescopes with the largest effective area.
58 thin nested mirror shells in each X-ray telescope.
Moderate and high spectral resolution.
Simultaneous optical/UV observations
Spatial resolution: 6”
Energy Range 0.2 to 12 keV
High Spectral resolution at LowE $E/\Delta E = 300$
Wide FoV

Comparison

A Comparison with other X-Ray Satellites

The following table compares XMM with selected previous X-ray satellites:

	ROSAT	ASCA	Chandra	XMM
Mirror effective area @ 1.0 keV (cm2)	400	350	800	4650
Imaging effective area @ 1.0 keV (cm2)	200	...	400	2400
Spectroscopy effective area @ 1.0 keV (cm2)	-	-	50	185 (orders 1+2)
Spectroscopic resolving power at 0.5 keV (E/dE)	(1)	9	400-1000	500
Mirror Resolution (arcsec)	3.5	73	0.2	6
CCD energy range (keV)	0.1-2.4	0.5-10	0.1-10	0.1-15
Orbit target visibility (hrs)	1.3	0.9	50	40

Chandra results

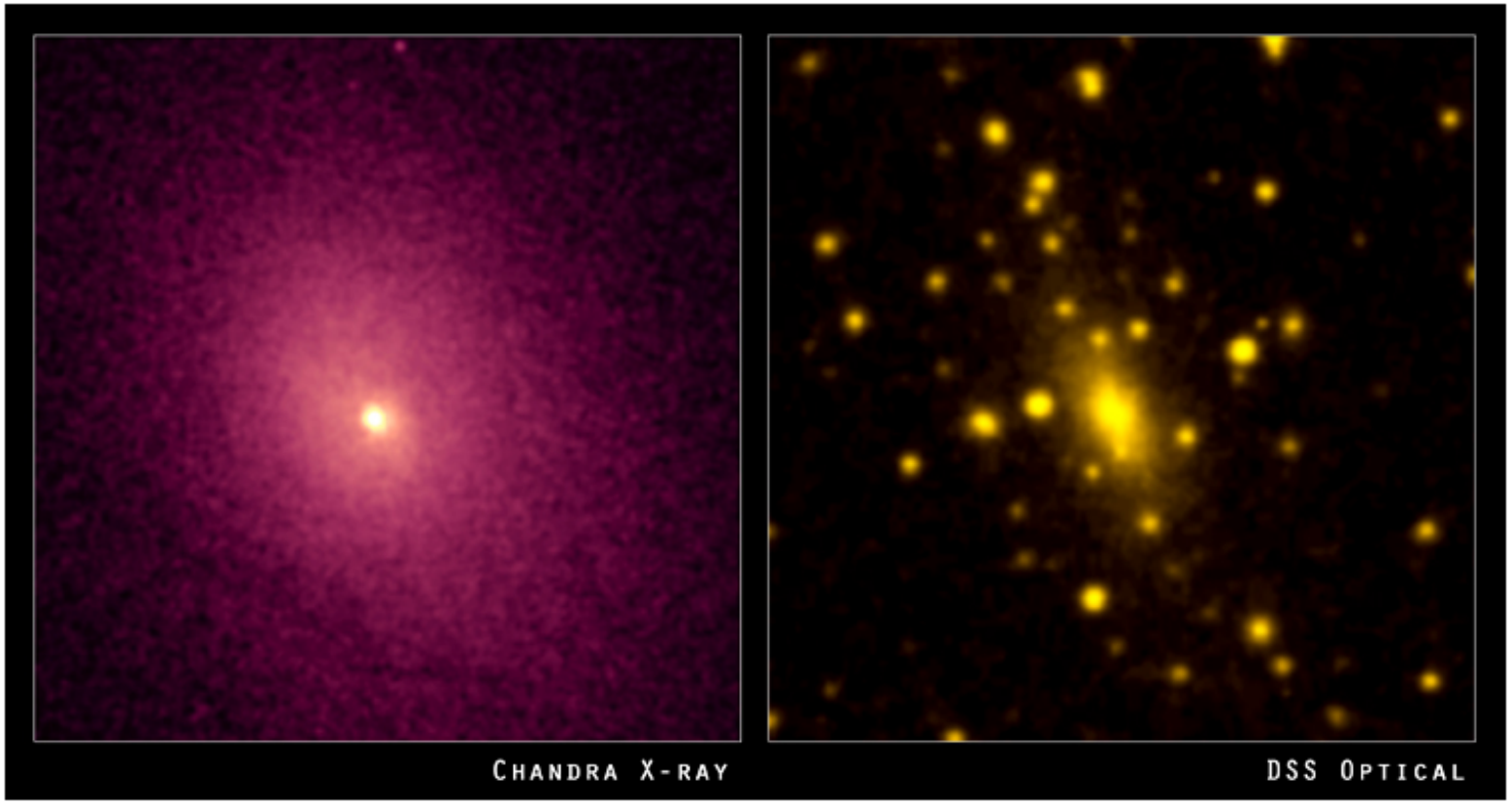

The galaxy cluster Abell 2029 is composed of thousands of galaxies (optical image) enveloped in a gigantic cloud of hot gas (X-ray image)

Chandra results

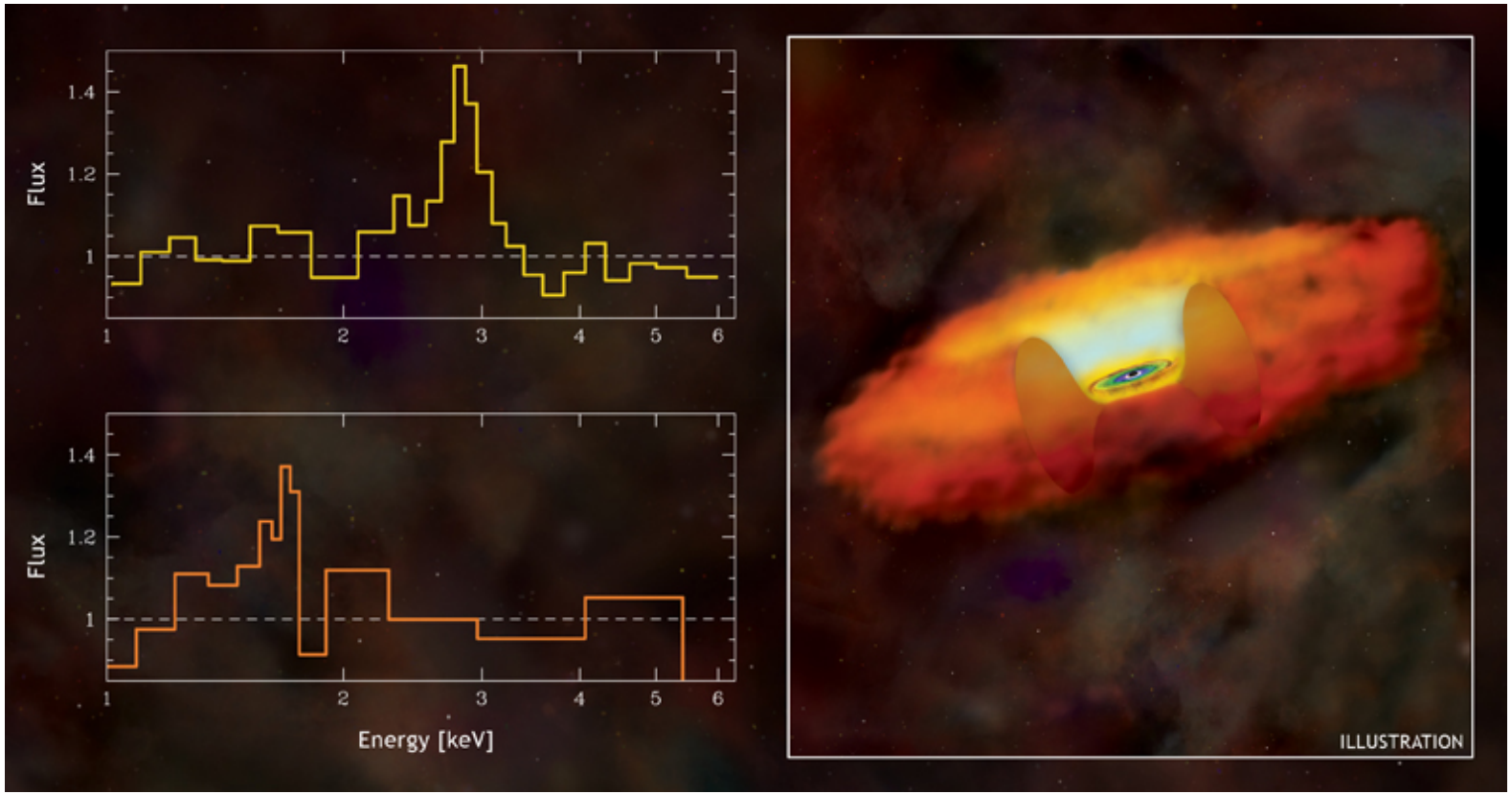

The left side of the above graphic shows portions of X-ray spectra from a subset of 50 black holes about 9 billion light years away (upper panel), and another group of 22 black holes that are about 11 billion light years away (lower panel).

Chandra results

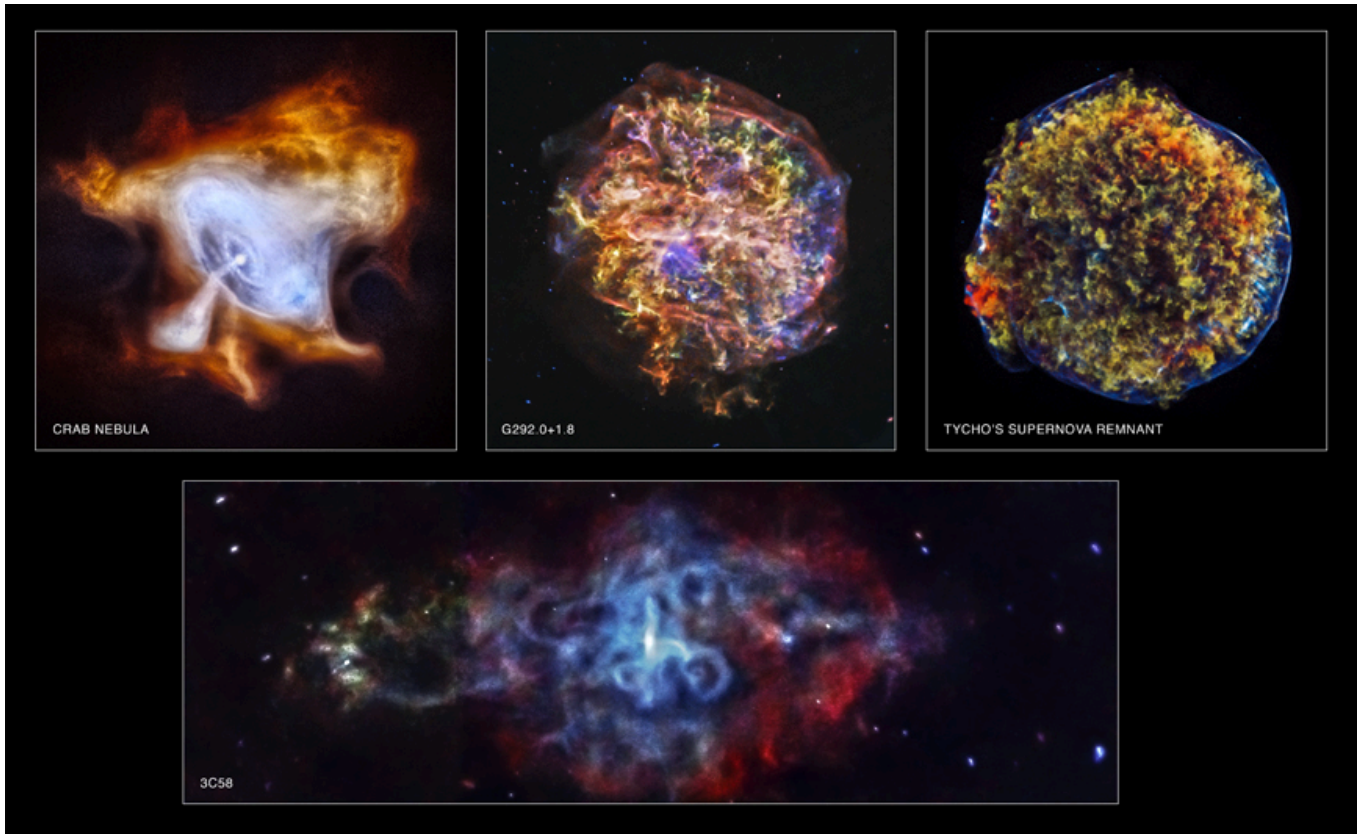

The Tycho and G292.0+1.8 supernova remnants show expanding debris from an exploded star and the associated shock waves.The images of the Crab Nebula and 3C58 show how neutron stars produced by a supernova can create clouds of high-energy particles.

XMM results

- The XXL project, the largest XMM-Newton observing programme to date, set itself the ambitious task of mapping galaxy clusters back to a time when the Universe was just half of its present age. Its aim was to trace the evolution of the large-scale structure of the Universe.

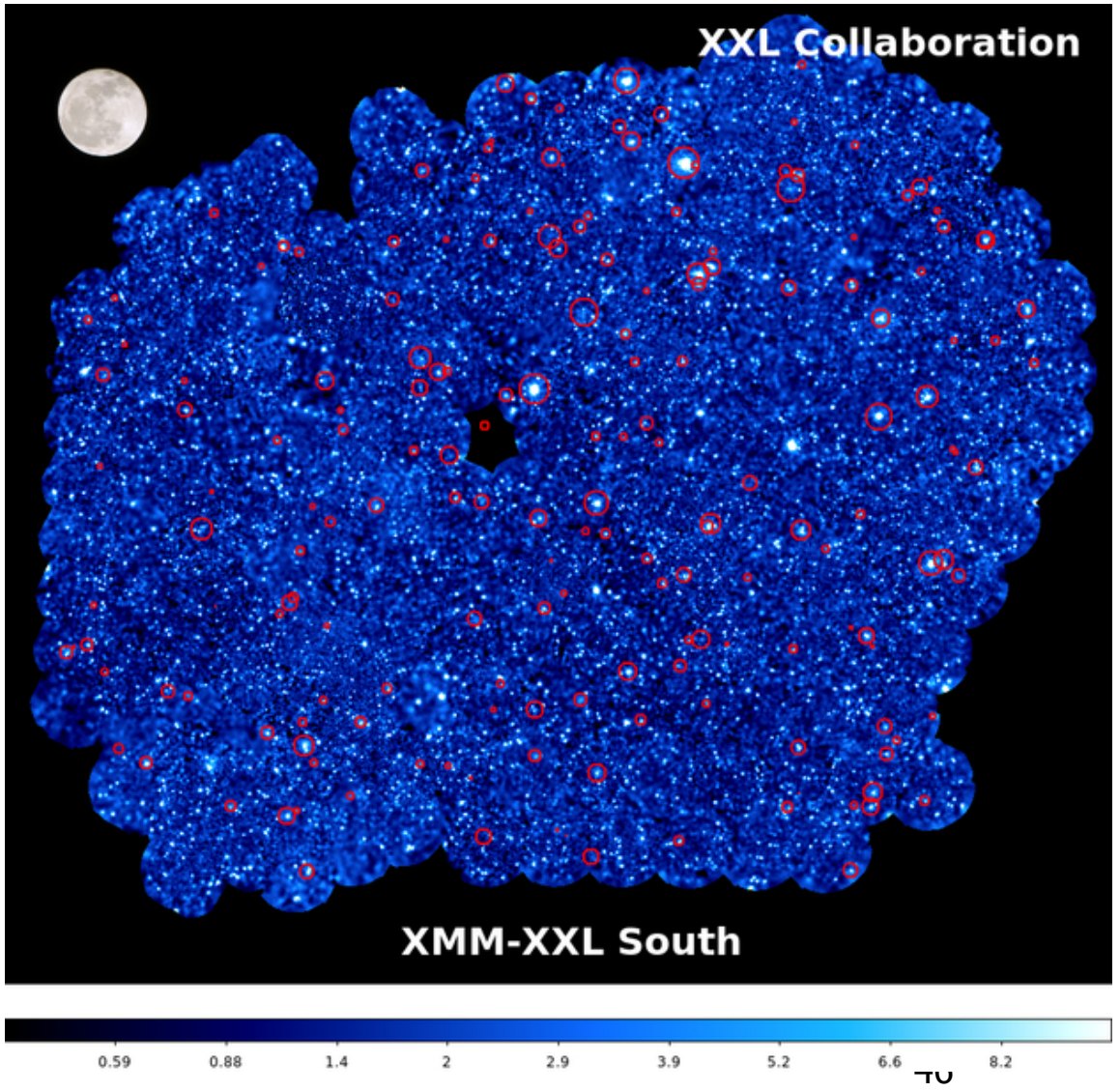

XMM results

Components of the galaxy cluster Abell 2744, also known as the Pandora Cluster: galaxies (white), hot gas (red) and dark matter (blue).

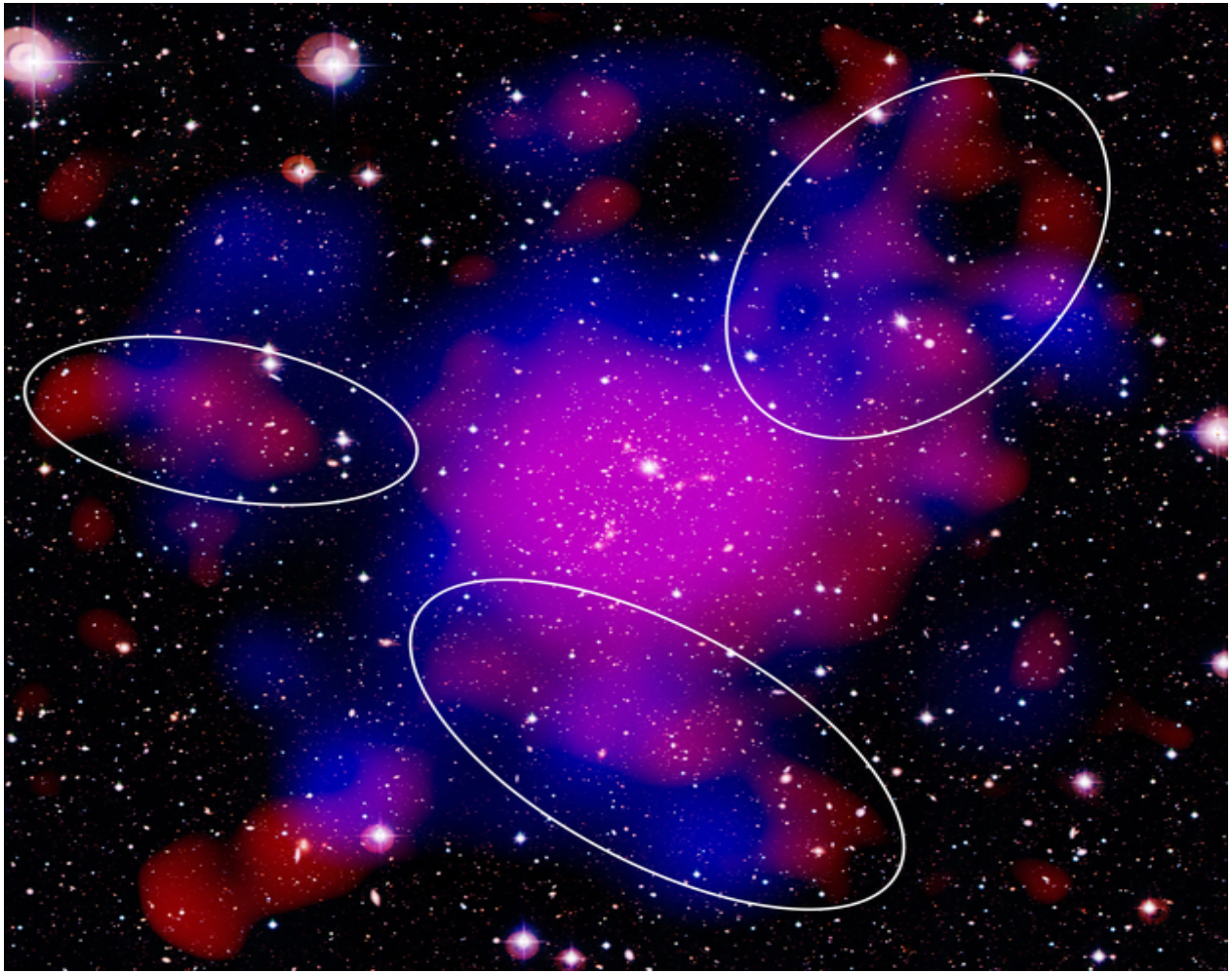

X-ray science highlights

Chandra Images by Category

Solar System (9 listings)
Comets and planets

Normal Stars & Star Clusters (30 listings)
Stellar coronas, clusters of stars and hot gas produced by outflow from young stars.

White Dwarfs & Planetary Nebulas (10 listings)
Hot gas associated with the final stages of evolution of Sun-like stars, novas, and other white dwarfs in binary star systems.

Supernovas & Supernova Remnants (34 listings)
X-ray sources produced by the violent explosions of massive stars.

Neutron Stars/X-ray Binaries (26 listings)
Hot, isolated neutron stars, rotation-powered pulsars, and neutron stars accreting matter from a nearby companion star.

Black Holes (27 listings)
Stellar black holes, mid-mass black holes, and supermassive black holes.

Milky Way Galaxy (14 listings)
Images related to the Galactic Center and other features of the structure and evolution of the Milky Way Galaxy.

Normal Galaxies & Starburst Galaxies (39 listings)
Images of spiral, elliptical, and irregular galaxies that show X-ray sources associated with collapsed stars and star formation.

Quasars & Active Galaxies (33 listings)
Galaxies with unusually energetic activity, including high-energy jets, that is related to a central supermassive black hole.

Groups & Clusters of Galaxies (33 listings)
Vast clouds of hot gas embedded with numerous galaxies.

Cosmology/Deep Fields/X-ray Background (13 listings)
The sky as observed in X-rays is not dark, but gives off a glow thought to be from many distant sources. Deep surveys with the Chandra X-ray Observatory should reveal the cause of this glow.

Miscellaneous (8 listings)
Objects that don't fit in the above categories, such as brown dwarfs & gamma-ray bursts.

X-ray science highlights

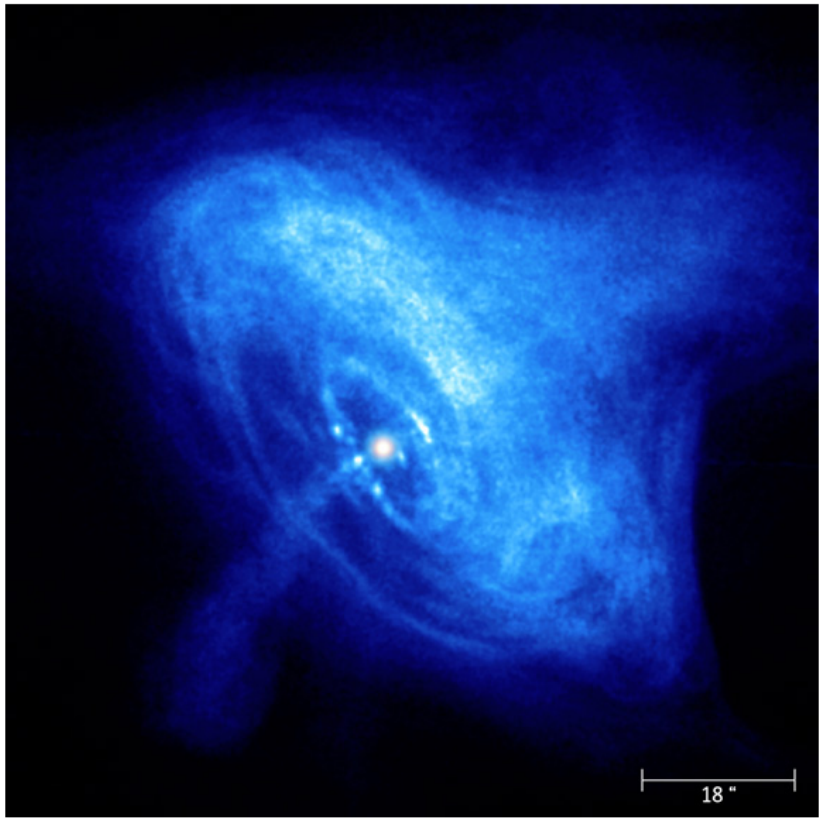

This image provides a view of the activity in the inner region around the Crab Nebula pulsar, a rapidly rotating neutron star seen as a bright white dot near the center of the images.

A wisp can be seen moving outward at half the speed of light from the upper right of the inner ring around the pulsar.
The wisp appears to merge with a larger outer ring that is visible in both X-ray and optical images.

The inner X-ray ring consists of about two dozen knots that form, brighten and fade. As a high-speed wind of matter and antimatter
particles from the pulsar plows into the surrounding nebula, it creates
a shock wave and forms the inner ring.
Energetic shocked particles move outward to
brighten the outer ring and produce an extended X-ray glow.

X-ray science highlights

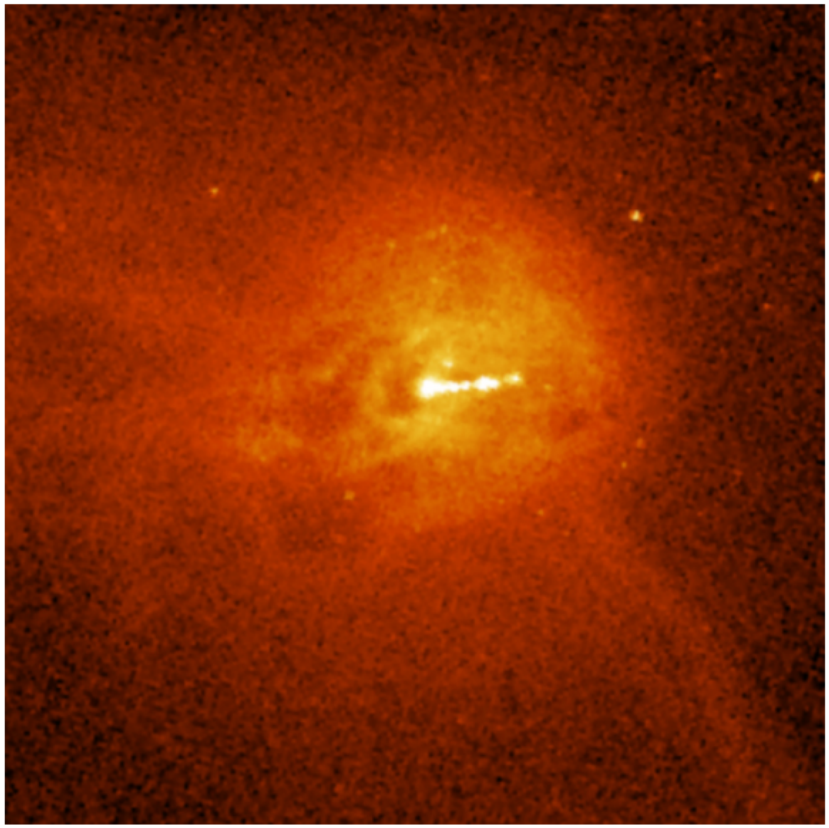

This close-up of M87 shows the region surrounding
the jet of high-energy particles in more detail.
The jet is thought to be pointed at a small angle to the
line of sight, out of the plane of the image.
This jet may be only the latest in a series of jets
that have been produced as magnetized
gas spirals in a disk toward the supermassive black hole

X-ray science highlights

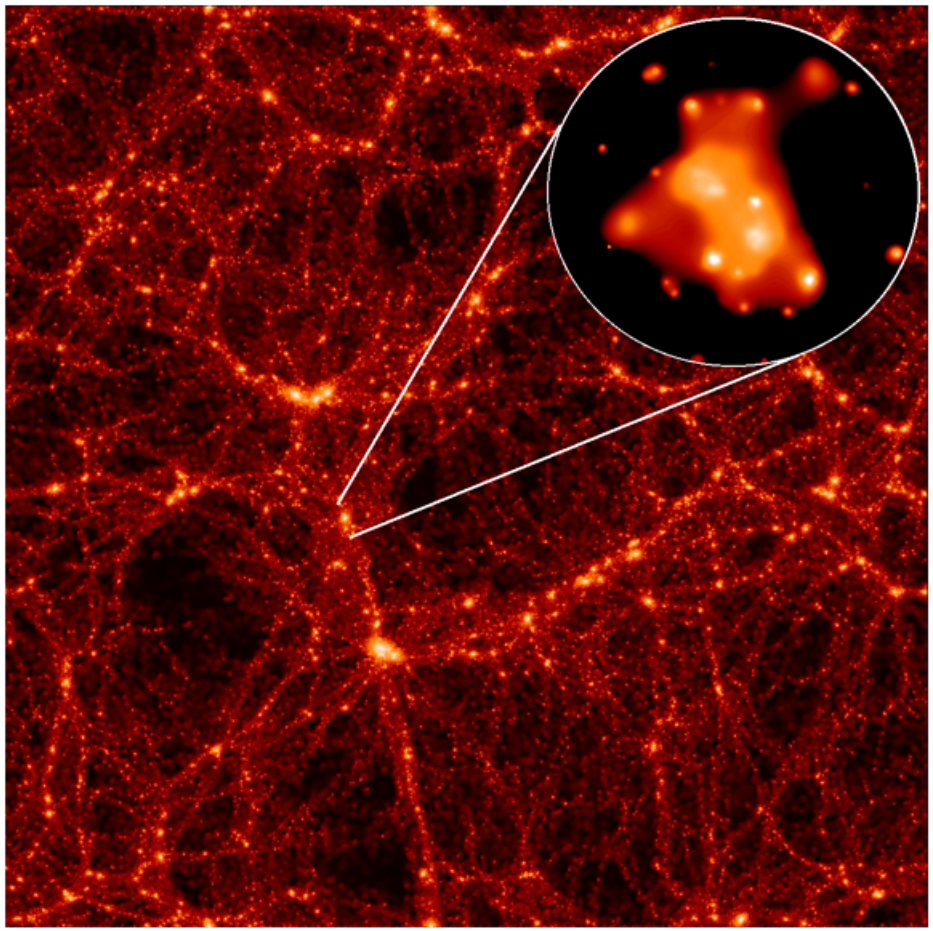

This image shows a computer simulation of a large volume of the Universe.
An XMM-Newton X-ray image of a real galaxy cluster from the study is superimposed to illustrate the formation of galaxy clusters in the densest parts of the universe.

Dark Matter and Cosmo Simulations

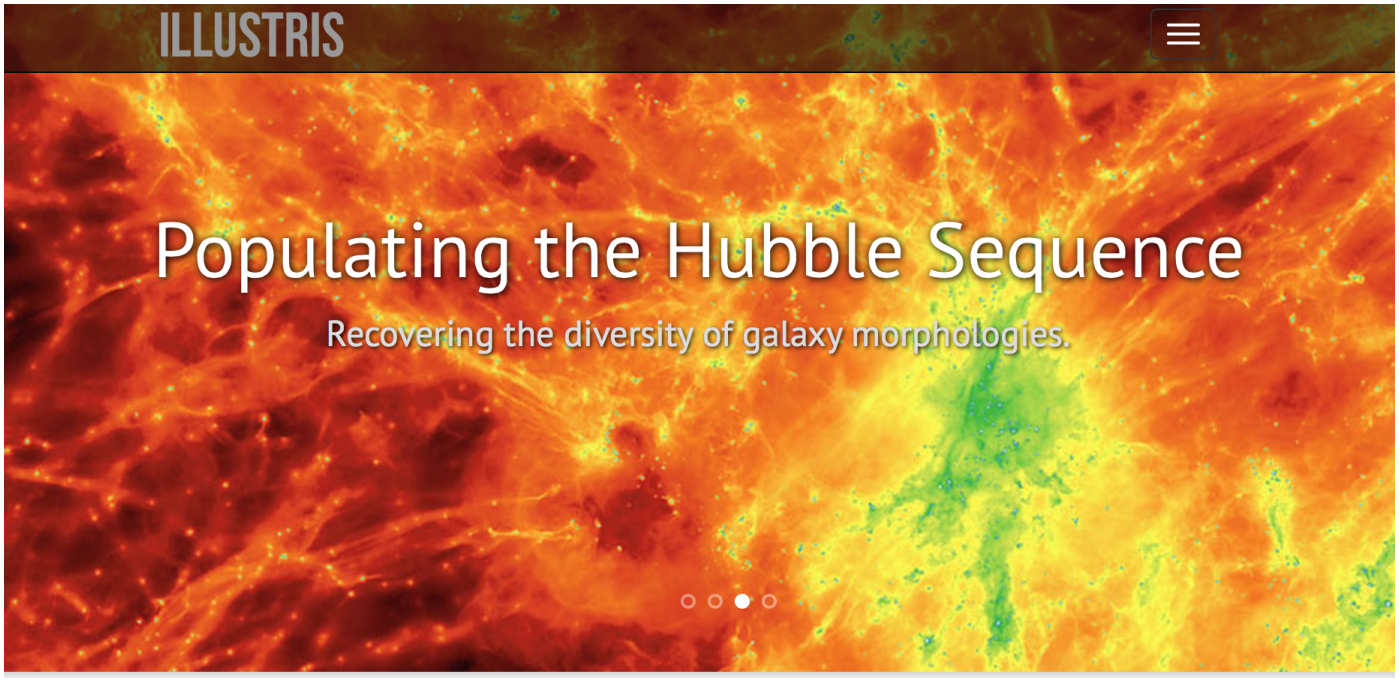

Welcome

The Illustris project is a large cosmological simulation of galaxy formation, completed in late 2013, using a state of the art numerical code and a comprehensive physical model. Building on several years of effort by members of the collaboration, the Illustris simulation represents an unprecedented combination of high resolution, total volume, and physical fidelity. The About page contains detailed descriptions of the project, for both the general public and researchers in the field.

On this website we present the scientific motivation behind the project, a list of the collaboration members, key results and references, movies and images created from the simulation data, information on upcoming public data access, and tools for interactive data exploration. The short video below is a compilation made from some of the movies available on the Media page.

http://www.illustris-project.org

http://www.tng-project.org

Dark Matter and Cosmo Simulations

Numerical Simulations of the Dark Universe: State of the Art and the Next Decade

Michael Kuhlen[a], Mark Vogelsberger[b], Raul Angulo[c,d]

[a] *Theoretical Astrophysics Center, University of California Berkeley, Hearst Field Annex, Berkeley, CA 94720, USA*
[b] *Hubble Fellow, Harvard-Smithsonian Center for Astrophysics, 60 Garden Street, Cambridge, MA 02138, USA*
[c] *Max-Planck-Institute for Astrophysics, Karl-Schwarzschild-Str. 1, 85740 Garching, Germany*
[d] *Kavli Institute for Particle Astrophysics and Cosmology, Stanford University, Menlo Park, CA 94025, USA*

Abstract

We present a review of the current state of the art of cosmological dark matter simulations, with particular emphasis on the implications for dark matter detection efforts and studies of dark energy. This review is intended both for particle physicists, who may find the cosmological simulation literature opaque or confusing, and for astro-physicists, who may not be familiar with the role of simulations for observational and experimental probes of dark matter and dark energy. Our work is complementary to the contribution by M. Baldi in this issue, which focuses on the treatment of dark energy and cosmic acceleration in dedicated N-body simulations.

Truly massive dark matter-only simulations are being conducted on national supercomputing centers, employing from several billion to over half a trillion particles to simulate the formation and evolution of cosmologically representative volumes (cosmic scale) or to zoom in on individual halos (cluster and galactic scale). These simulations cost millions of core-hours, require tens to hundreds of terabytes of memory, and use up to petabytes of disk storage. Predictions from such simulations touch on almost every aspect of dark matter and dark energy studies, and we give a comprehensive overview of this connection. We also discuss the limitations of the cold and collisionless DM-only approach, and describe in some detail efforts to include different particle physics as well as baryonic physics in cosmological galaxy formation simulations, including a discussion of recent results highlighting how the distribution of dark matter in halos may be altered. We end with an outlook for the next decade, presenting our view of how the field can be expected to progress.

http://arxiv.org/pdf/1209.5745v2.pdf

Suzaku

- Suzaku launched on July 10, 2005. Before launch it was called Astro-E2, and the name was changed to Suzaku shortly after the successful launch.
- Suzaku's four CCD cameras for low-energy X-rays and detector for high-energy X-rays continue to study the X-ray sky. In scientists' words, Suzaku is designed for "broad-band, high-sensitivity, high-resolution" spectroscopy.

http://www.isas.jaxa.jp/e/enterp/missions/suzaku/

NuSTAR

- The NuSTAR (Nuclear Spectroscopic Telescope Array) mission has deployed the first orbiting telescopes to focus light in the high energy X-ray (3 - 79 keV) region of the electromagnetic spectrum. Our view of the universe in this spectral window has been limited because previous orbiting telescopes have not employed true focusing optics, but rather have used coded apertures that have intrinsically high backgrounds and limited sensitivity.

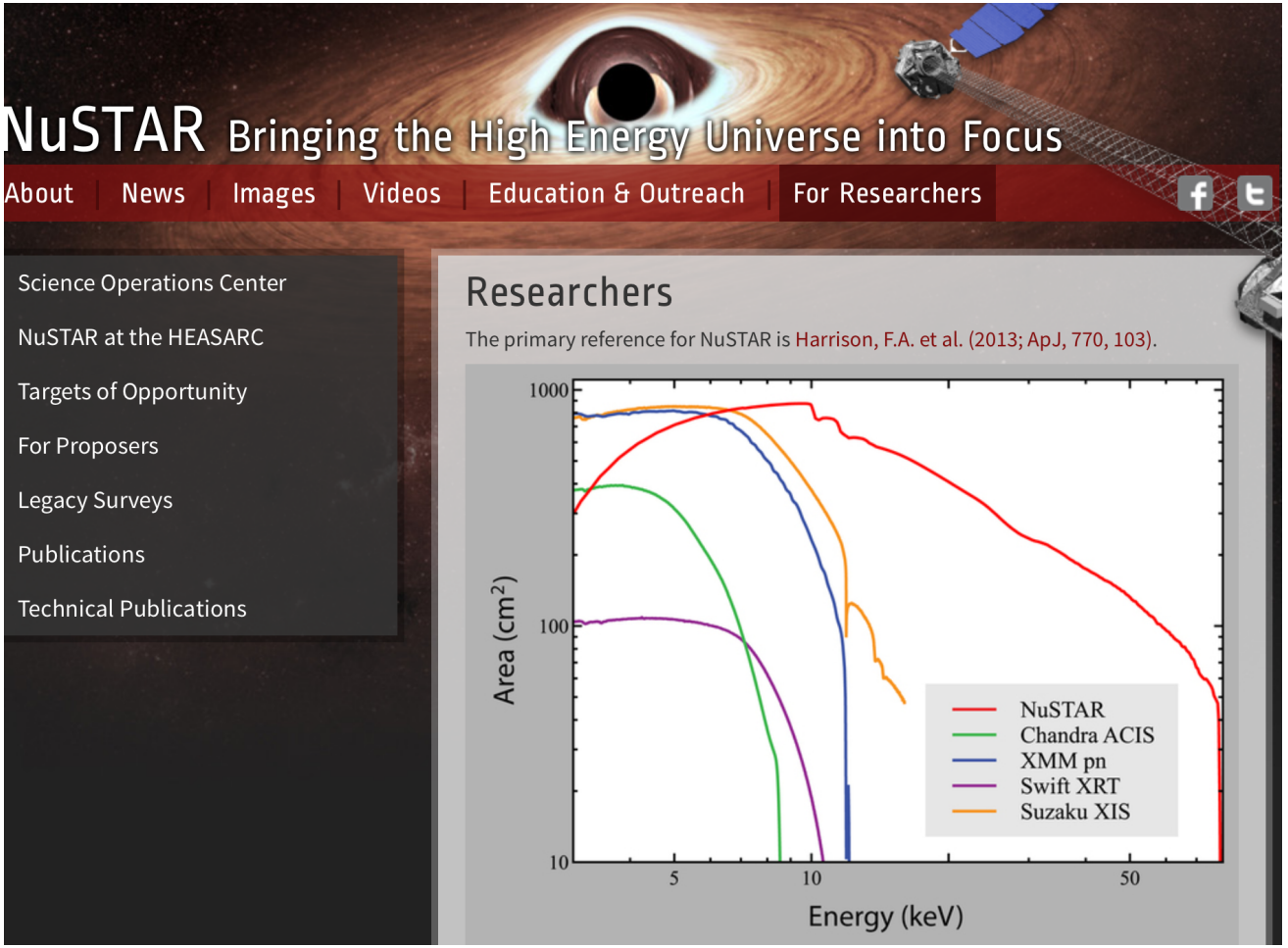

http://www.nustar.caltech.edu/

MAXI

The Monitor of All-sky X-ray Image, MAXI, is the first experiment installed on the Japanese Experiment Module Exposed Facility (JEM-EF or Kibo-EF) on the International Space Station (ISS) and the first high energy astrophysical experiment placed on the space station.

The main objectives of MAXI are early detection of X-ray transient events, and monitoring the intensity fluctuation of known X-ray sources over long periods by scanning the all sky in soft and hard X-ray.

- two semi-circular arc-shaped X-ray slit cameras with wide FOVs. In the 92 minutes it takes the ISS to orbit the earch, MAXI gets a 360 deg image of the entire sky.
- two kinds of X-ray detectors, collecting events from the slit cameras: a gas proportional counters, the Gas Slit Camera (GSC; 2-30 keV), and a X-ray CCD, Solid-state Slit Camera (SSC; 0.5-12 keV).

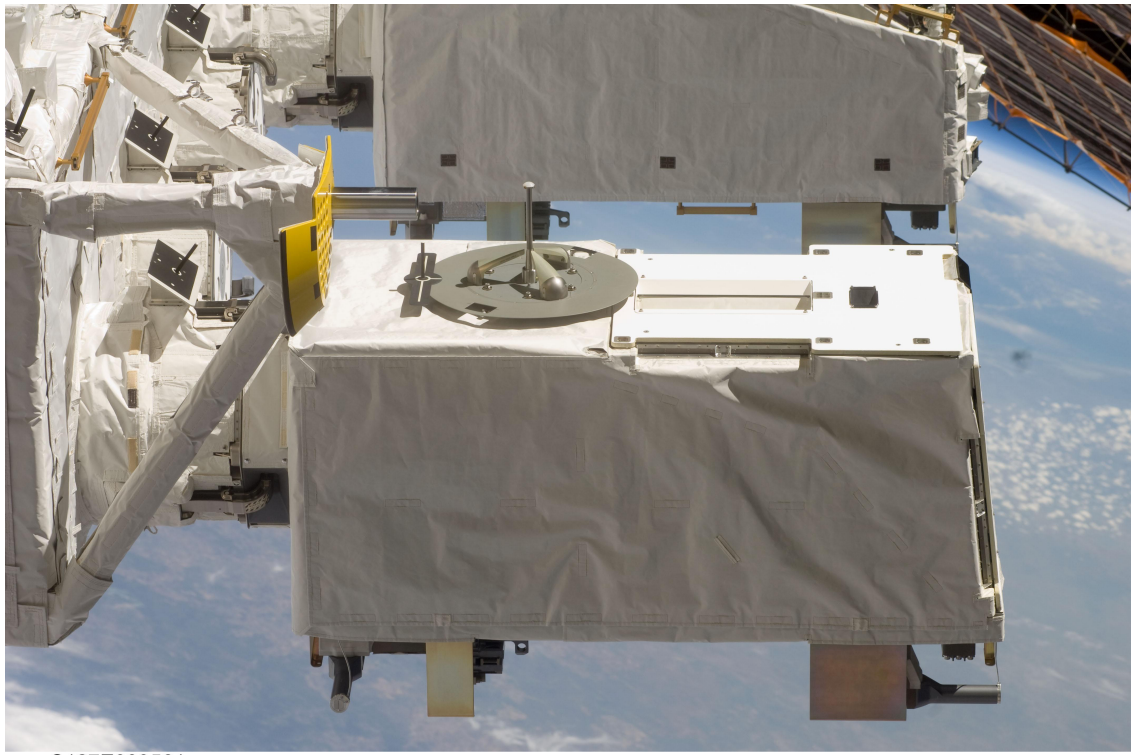

S127E009561

https://heasarc.gsfc.nasa.gov/docs/maxi/

Astro-H – Hitomi

http://astro-h.isas.jaxa.jp/en/

Astro-H – Hitomi

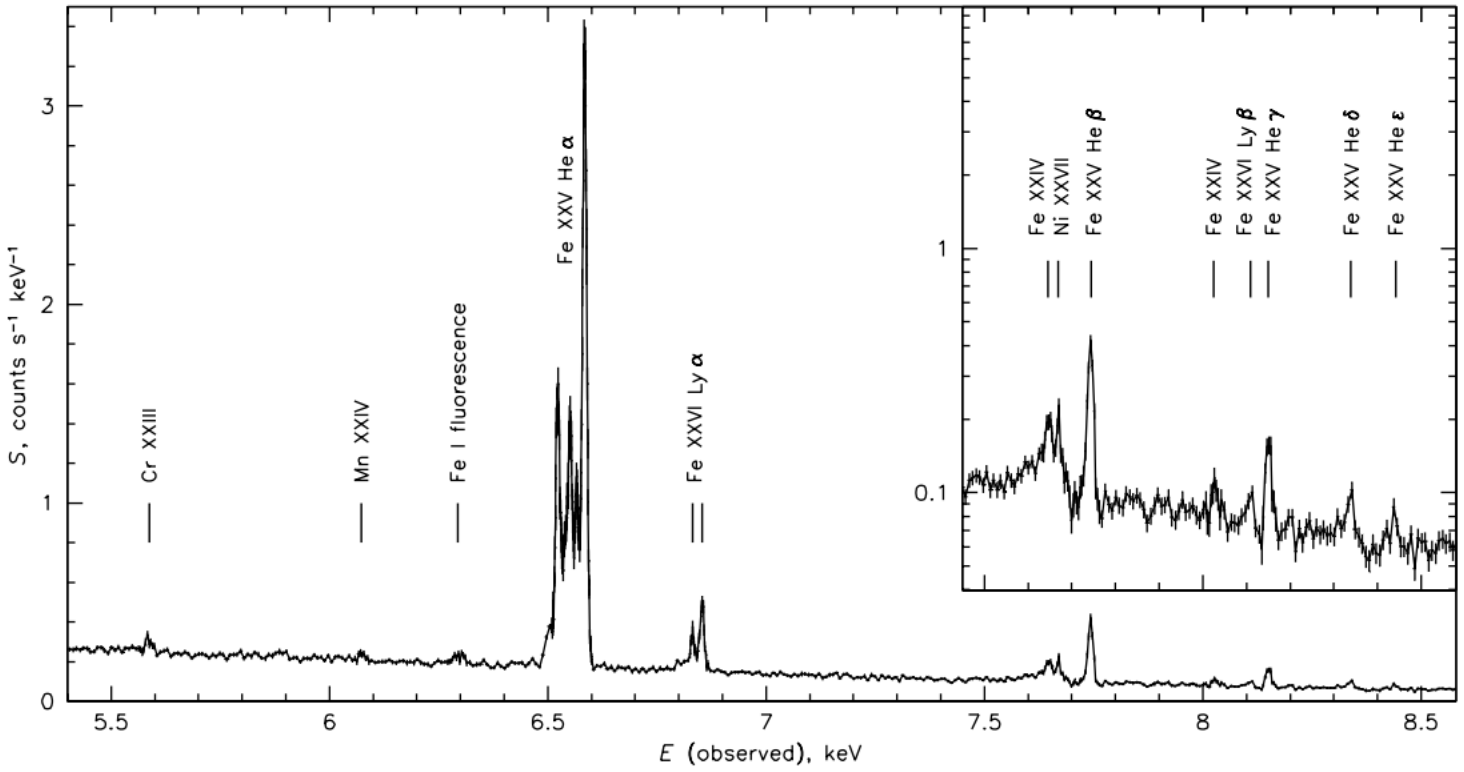

https://arxiv.org/pdf/1607.04487.pdf

XRISM

About XRISM | What's New | Timelines/Events | Results | Documentation | Related Sites | Gallery

About XRISM

The X-ray Imaging and Spectroscopy Mission (XRISM) is a JAXA/NASA collaborative mission, with ESA participation, with the objective to investigate X-ray celestial objects in the Universe with high-throughput, high-resolution spectroscopy. XRISM is expected to launch in the Japanese fiscal year 2022 (TBR) on a JAXA H-IIA rocket.

https://heasarc.gsfc.nasa.gov/docs/xrism/

NICER

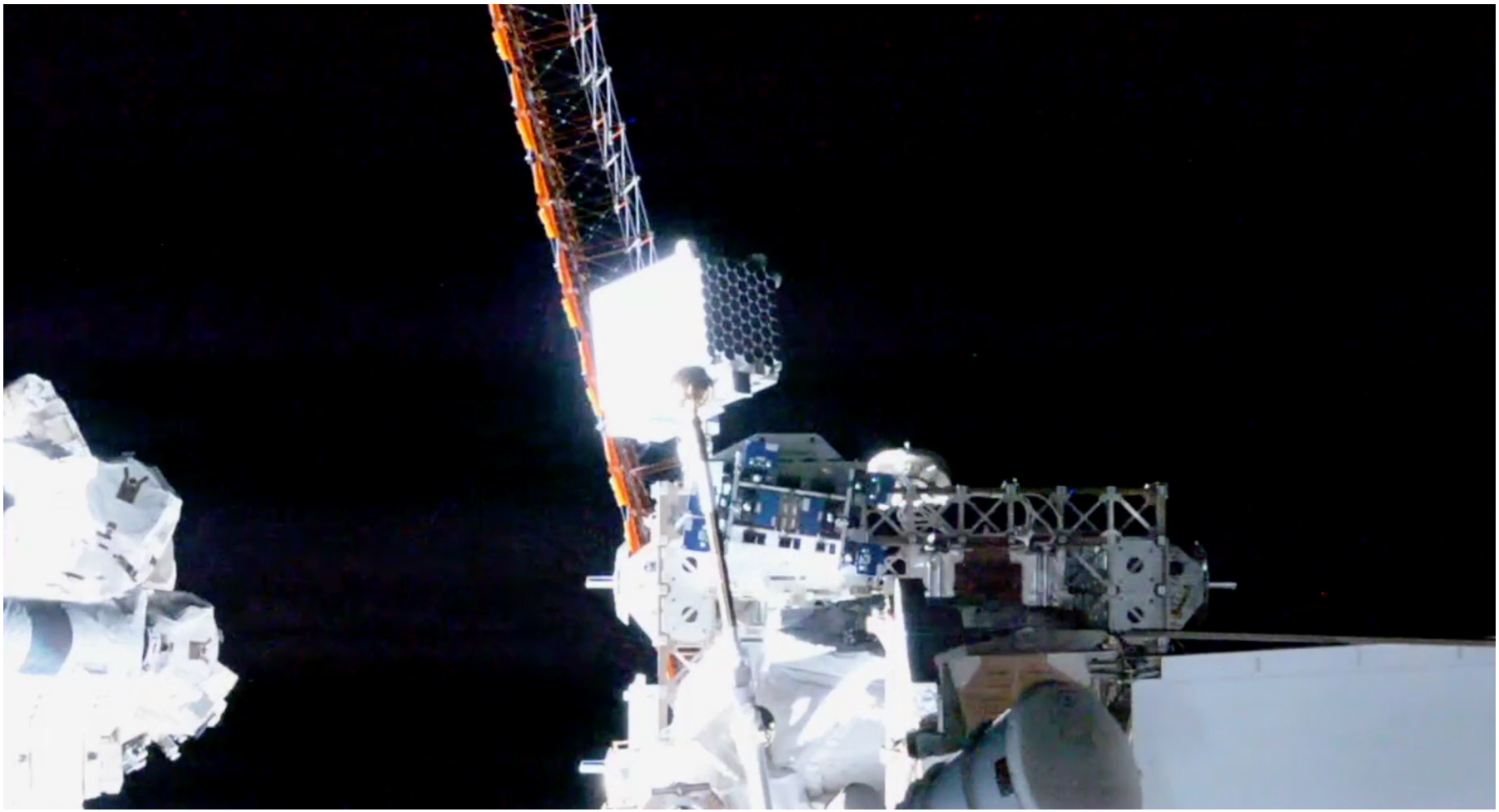

https://heasarc.gsfc.nasa.gov/docs/nicer/

ASTROSAT

https://www.isro.gov.in/Spacecraft/astrosat

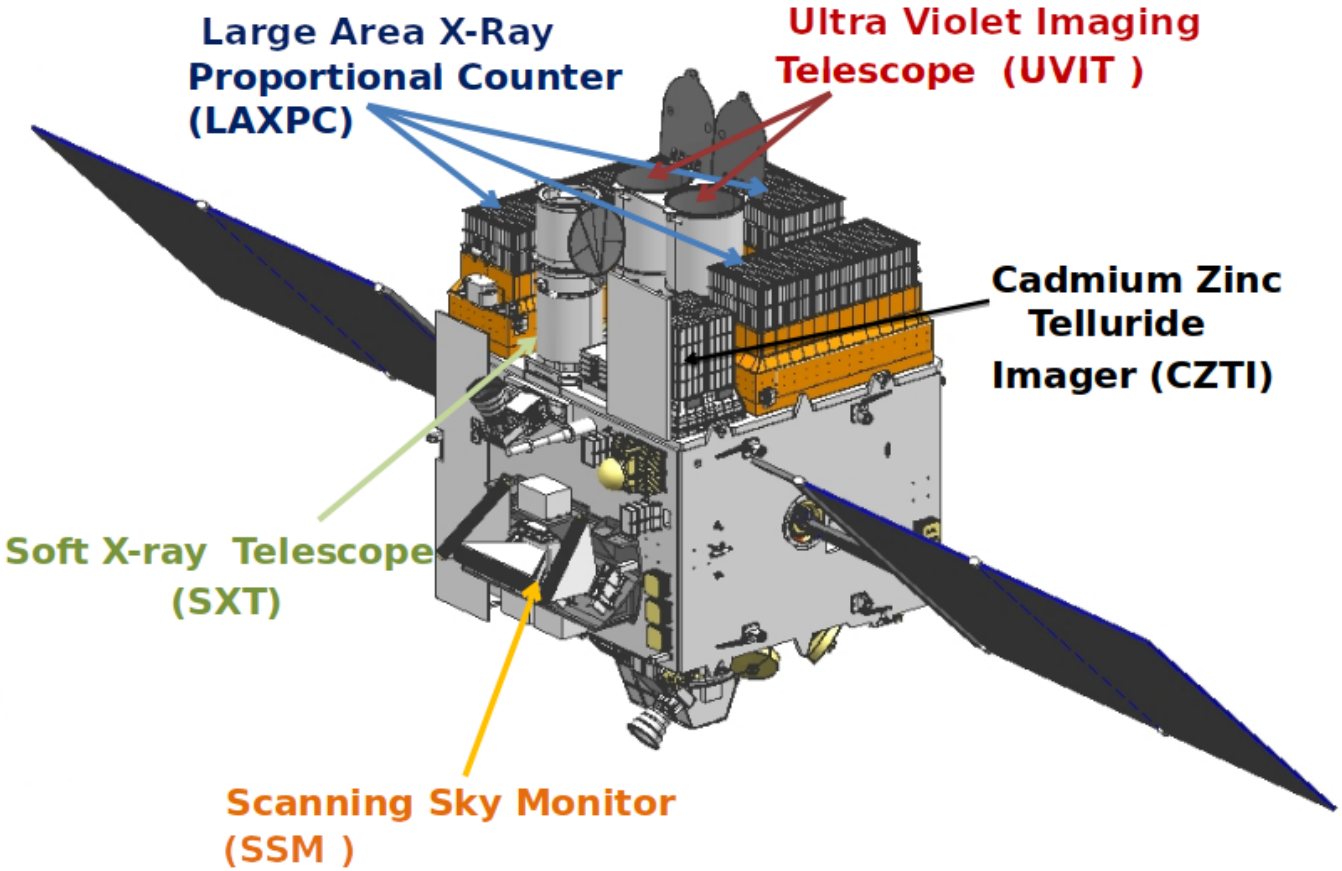

https://astrobrowse.issdc.gov.in/astro_archive/archive/Home.jsp

HMXT

http://www.hxmt.org/index.php/enhome

eROSITA

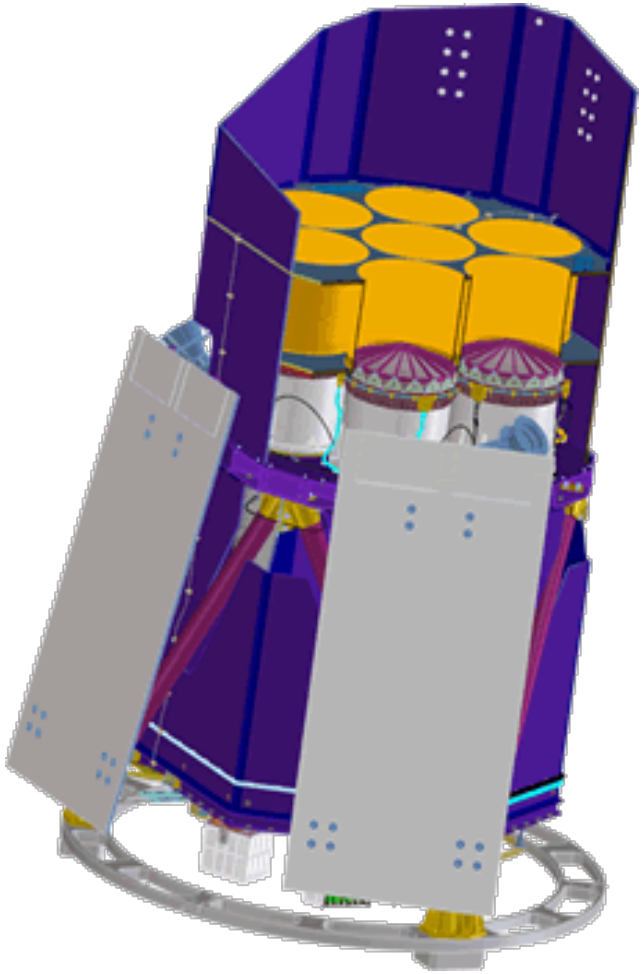

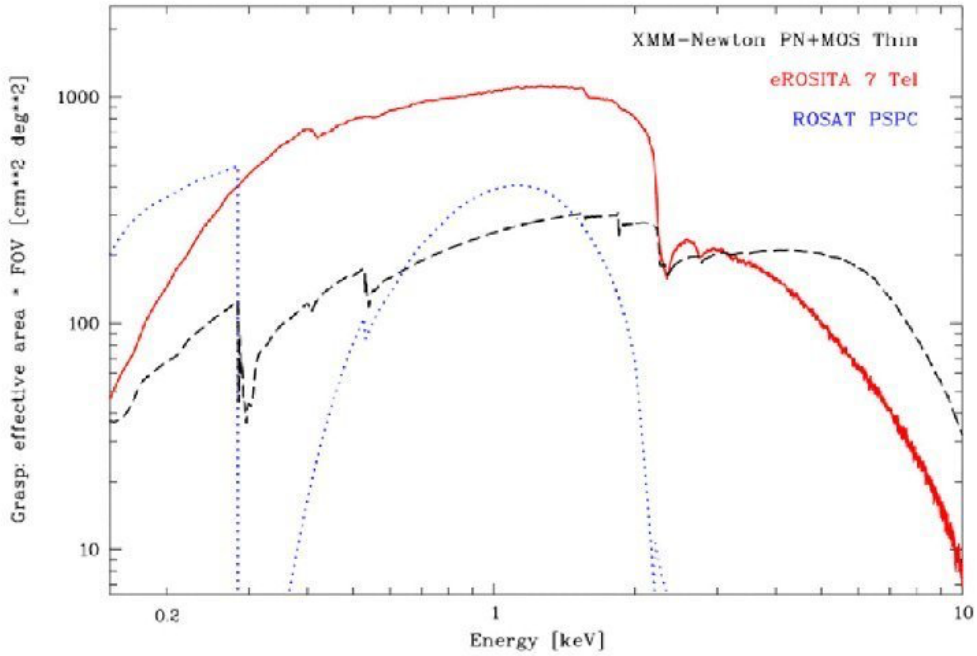

https://www.mpe.mpg.de/eROSITA

IXPE

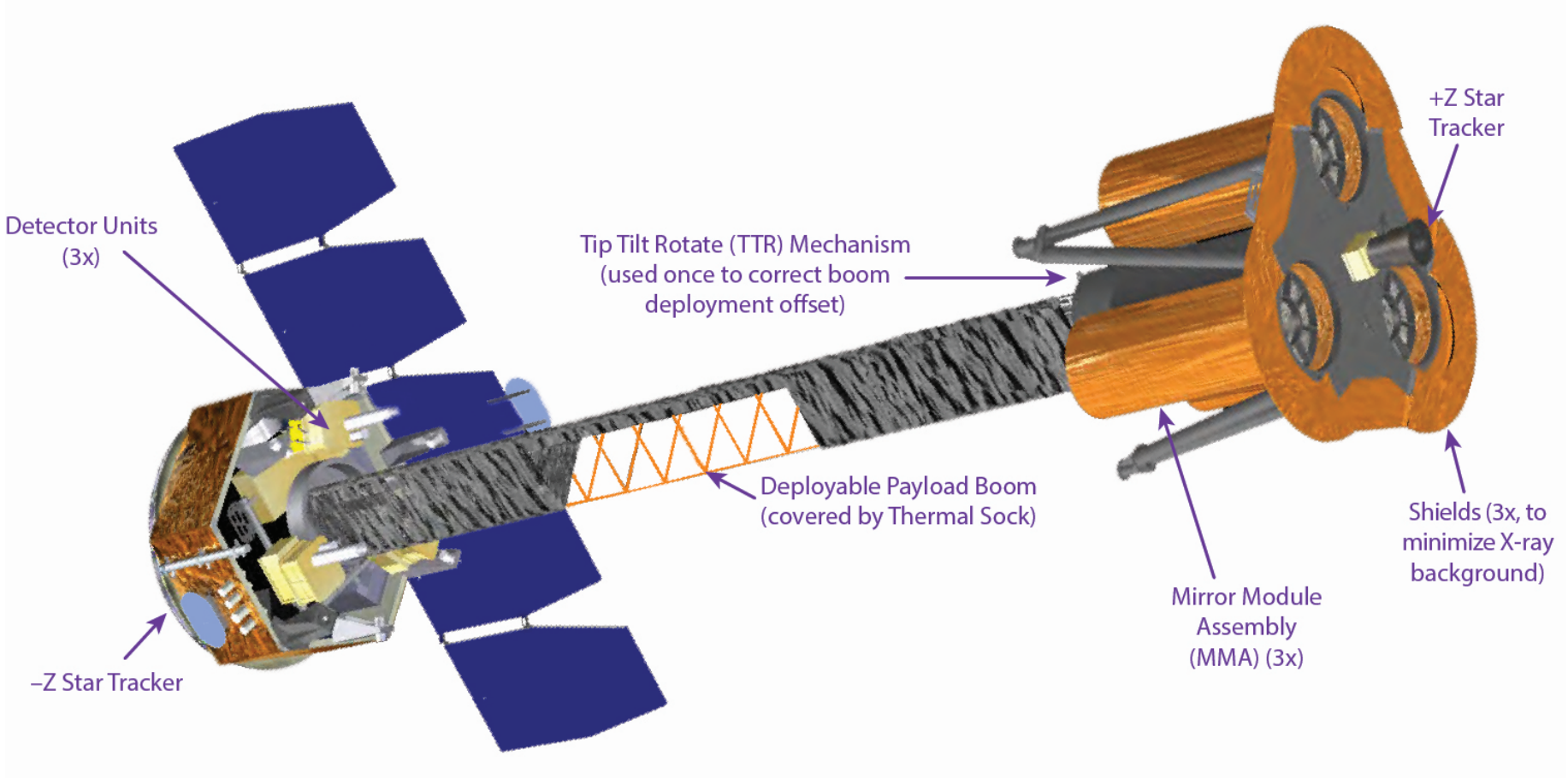

https://wwwastro.msfc.nasa.gov/ixpe/

IXPE

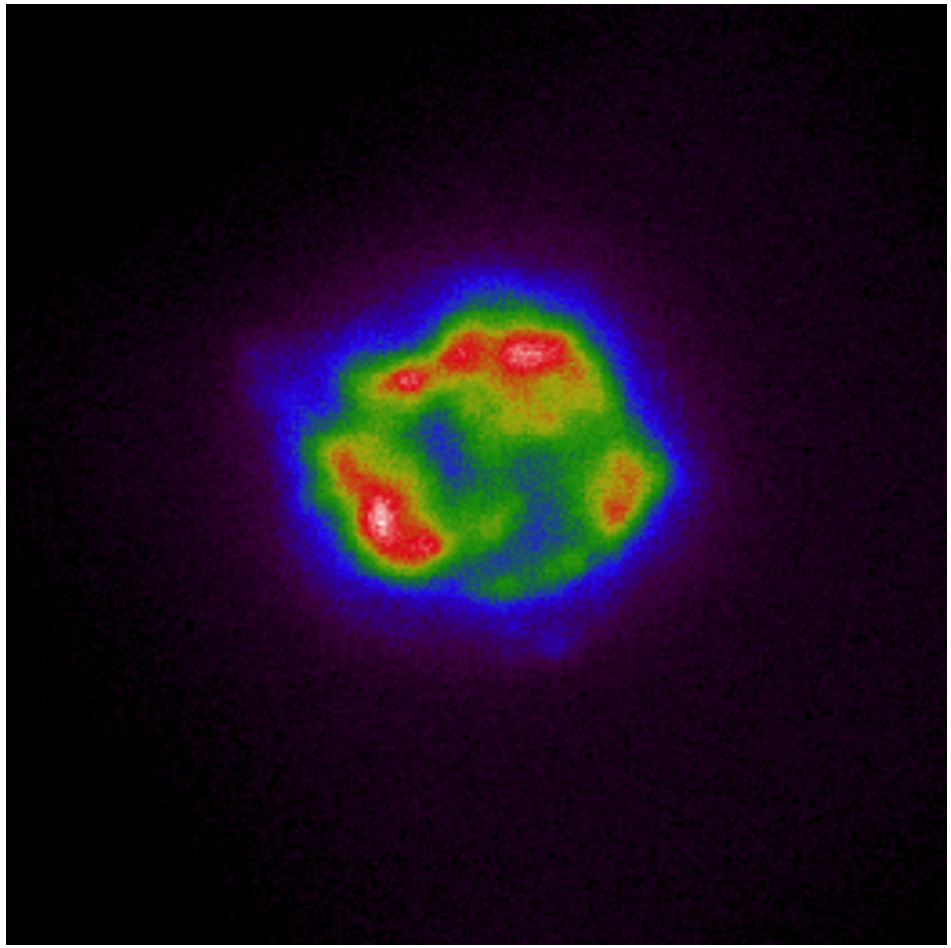

https://www.nasa.gov/mission_pages/ixpe/news/nasa-s-ixpe-sends-first-science-image.html

XIPE

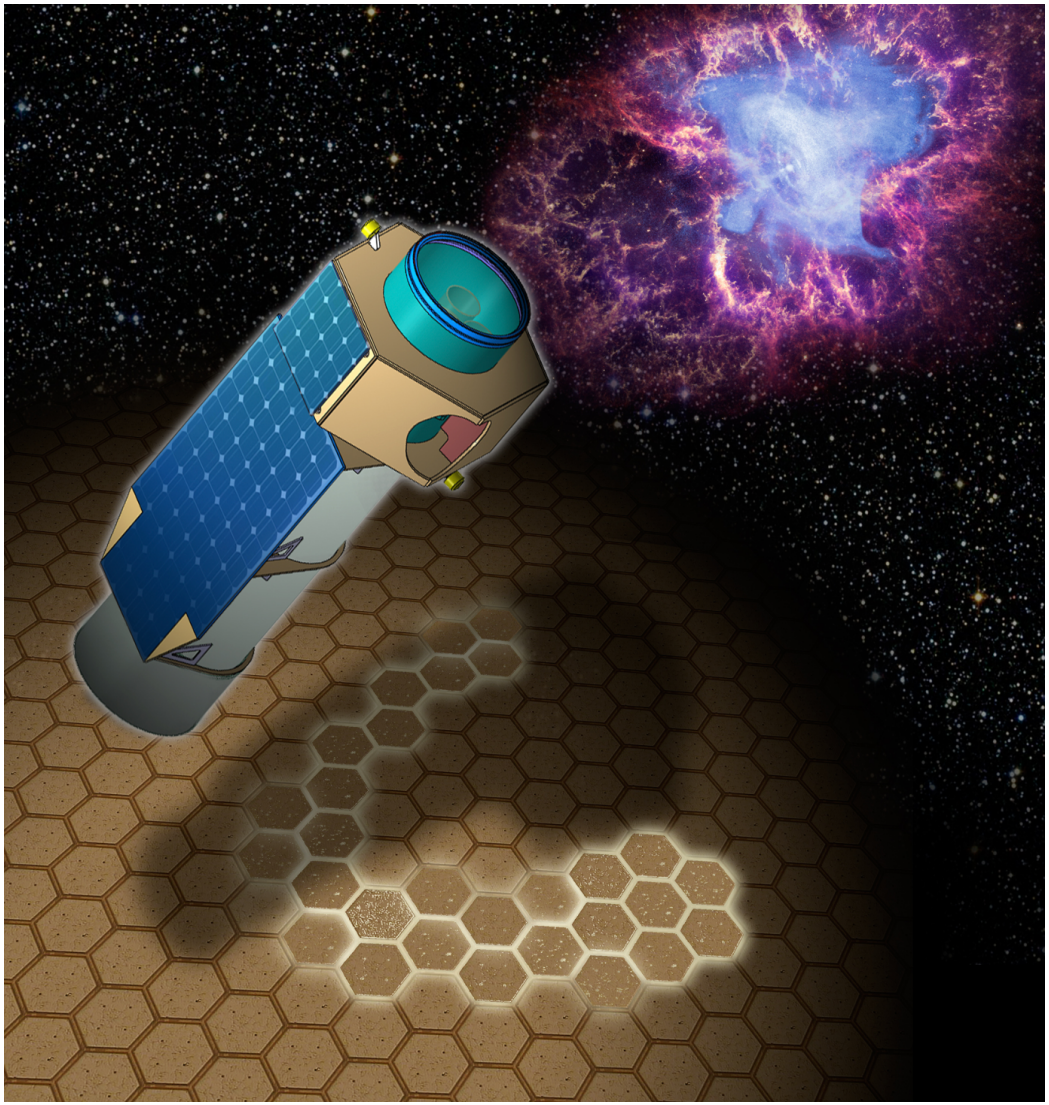

http://www.isdc.unige.ch/xipe/

LOFT

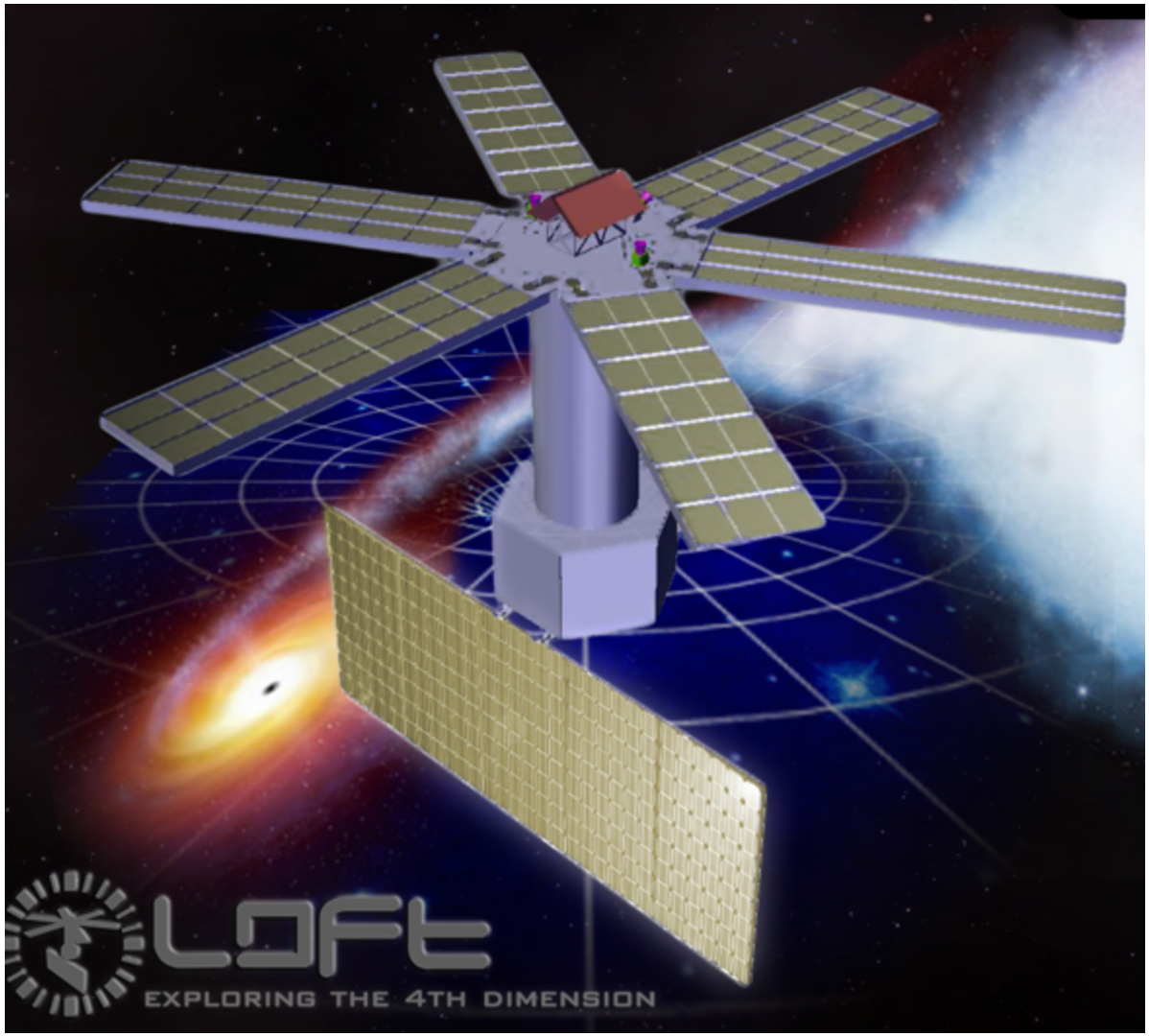

http://www.isdc.unige.ch/loft/

eXTP

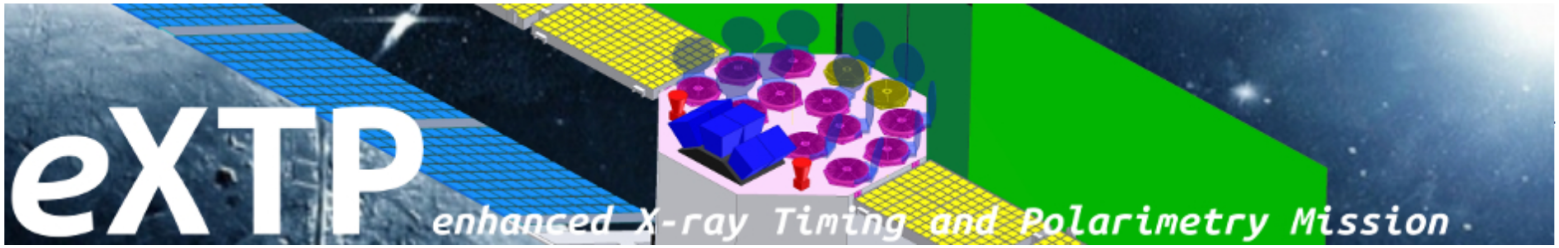

The eXTP Mission

The eXTP mission
The eXTP Payload
Science with eXTP
SPIE 2016 paper
Publications on eXTP
Public Response Files

eXTP Teams

WG1 - Dense Matter
WG2 - Strong Field Gravity
WG3 - Strong Magnetism
WG4 - Observatory Science
WG5 - Synergy with GWs
WG6 - Simulations
Instrument Working Group
Consortium

The eXTP Mission

The enhanced X-ray Timing and Polarimetry mission (eXTP) is a science mission designed to study the state of matter under extreme conditions of density, gravity and magnetism. Primary goals are the determination of the equation of state of matter at supra-nuclear density, the measurement of QED effects in highly magnetized star, and the study of accretion in the strong-field regime of gravity. Primary targets include isolated and binary neutron stars, strong magnetic field systems like magnetars, and stellar-mass and supermassive black holes.

The mission carries a unique and unprecedented suite of state-of-the-art scientific instruments enabling for the first time ever the simultaneous spectral-timing-polarimetry studies of cosmic sources in the energy range from 0.5-30 keV (and beyond). Key elements of the payload are:

- **the Spectroscopic Focusing Array** (**SFA**): a set of 11 X-ray optics operating in the 0.5-10 keV energy band with a field-of-view (FoV) of 12 arcmin each and a total effective area of ~0.9 m^2 and 0.6 m^2 at 2 keV and 6 keV respectively. The telescopes are equipped with Silicon Drift Detectors offering <180 eV spectral resolution.
- **the Large Area Detector** (**LAD**): a deployable set of 640 Silicon Drift Detectors, achieving a total effective area of ~3.4 m^2 between 6 and 10 keV. The operational energy range is 2-30 keV and the achievable spectral resolution better than 250 eV. This is a non-imaging instrument, with the FoV limited to <1° FWHM by the usage of compact capillary plates.
- **the Polarimetry Focusing Array** (**PFA**): a set of 2 X-ray telescope, achieving a total effective area of 250 cm^2 at 2 keV, equipped with imaging gas pixel photoelectric polarimeters. The FoV of each telescope is 12 arcmin and the operating energy range is 2-10 keV.
- **the Wide Field Monitor** (**WFM**): a set of 3 coded mask wide field units, equipped with position-sensitive Silicon Drift Detectors, covering in total a FoV of 3.7 sr and operating in the energy range 2-50 keV.

http://www.isdc.unige.ch/extp/

Athena

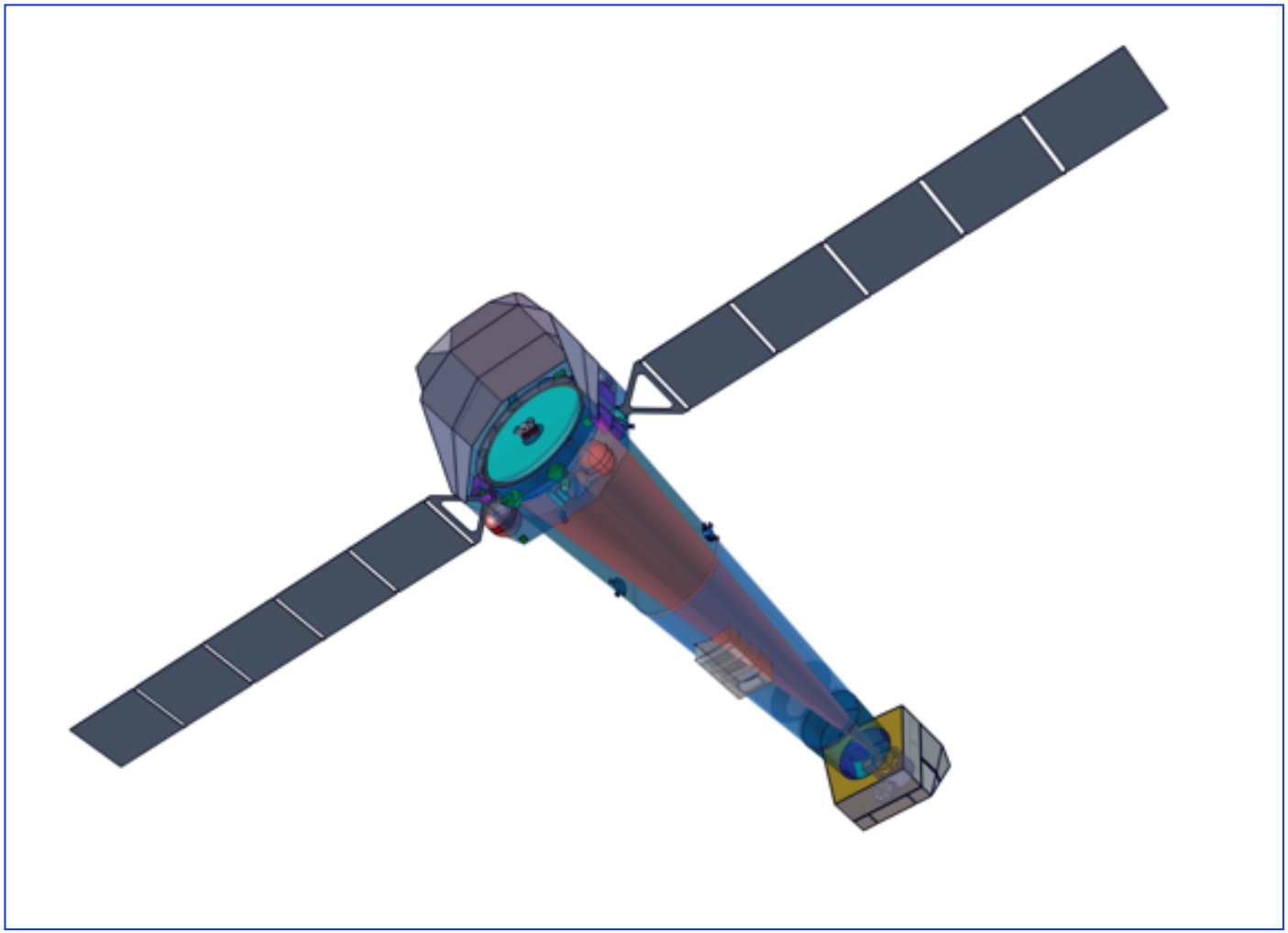

https://www.the-athena-x-ray-observatory.eu